Tectonophysics 821 (2021) 229146

Contents lists available at ScienceDirect

Tectonophysics

journal homepage: www.elsevier.com/locate/tecto

Imaging the roots of a post-collisional pluton: Implications for the voluminous Cambrian magmatism in the Araçuaí orogen (Brazil)

G.F. Souza Junior [a,*], R.I.F. Trindade [a], F.A. Temporim [a], U.D. Bellon [a], L.P. Gouvêa [b], C. C. Soares [c], C.A.D. Amaral [a], V. Louro [d]

[a] Instituto de Astronomia, Geofísica e Ciências Atmosféricas, Departamento de Geofísica, Universidade de São Paulo, São Paulo, Brazil
[b] Departamento de Geologia, Universidade Federal do Rio de Janeiro, Rio de Janeiro, Brazil
[c] Departamento de Geologia, Universidade Federal do Espírito Santo, Alegre, Brazil
[d] Instituto de Geociências, Universidade de São Paulo, São Paulo, Brazil

ARTICLE INFO

Keywords:
Araçuaí orogen
Post-collisional magmatism
Anisotropy of magnetic susceptibility
Gravity modelling
Microstructural analysis
Reverse diapirism

ABSTRACT

The Cambrian Santa Angélica intrusive complex (SAIC - SE, Brazil), is composed of two lobes with concentric fabric and bull's eyes shapes, each lobe containing a mafic nuclei and granitic borders. It intruded during the post-collisional phase of the Araçuaí orogen (AO). Although SAIC'S internal structure is described as exclusively magmatic, prominent solid-state deformation occurs at its borders, as well as an internal shear zone (ISZ). We studied the mechanisms that caused the different architectures displayed by the post-collisional bodies when emplaced in distinct crustal levels across the AO. We forward-modelled gravity data from the SAIC and its country rocks and performed structural analysis through anisotropy of magnetic susceptibility (AMS) and microstructural data of oriented thin sections in the SAIC border and the intrusion's country rocks. Magnetic measurements indicates that multidomain magnetite and pyrrhotite control the magnetic fabric of SAIC's country rocks. 2D gravity modelling shows that the northeast lobe outcrops its roots and its thickness is less than half of the southwest one. Three zones have been identified based on the occurrence of the solid-state microstructures: the country rocks and the border of the pluton display higher temperatures solid-state microstructures, overlapped by lower temperature ones, while the ISZ only shows high temperature structures. We suggest the SAIC experienced a reverse diapiric mechanism caused by the negative buoyancy of its mafic nuclei during crystallization. As the mafic cores sink through a ductile and hot halo in midcrust conditions, they deform the granitic rocks at the borders, as well as the country rocks, also generating the internal shear zone by the relative motion observed between the lobes. Furthermore, we infer that the buoyancy of the mafic and felsic magmas, together with crustal rheology, were the main constraints responsible to restrain the emplacement depth of the post-collisional plutons in the AO.

1. Introduction

The Araçuaí-West Congo orogen is an important orogenic system present in southeastern Brazil and West Africa (Alkmim et al., 2006), characterized by a voluminous and longstanding magmatism encompassing different tectonic phases, from pre-collisional to post-collisional magmatism (ca. 630 to 480 Ma) (De Campos et al., 2016; Pedrosa-Soares et al., 2011; Pedrosa-Soares and Wiedemann-Leonardos, 2000). Post-collisional plutons of the southern and northern portions of the orogen have contrasting shapes and structures. In the south they are usually small balloon-like bodies with inverse zoning and magma mixing/mingling features, related to the interaction between mantle and crustal derived magmas (Bayer et al., 1987; De Campos et al., 2004, 2016; Pedrosa-Soares et al., 2011; Pedrosa-Soares and Wiedemann-Leonardos, 2000; Wiedemann et al., 2002). Recent studies integrating analysis of the magnetic fabric with microstructural data (Bellon et al., 2021; Temporim et al., 2020a), highlight the internal concentric pattern of the magnetic foliation in these plutons, which is decoupled from the regional structural trend. A shallower portion of the crust outcrops in the northern region of the orogen when compared to the southern region. In the north the post-collisional plutons are represented by much larger batholith intrusions, consisting of granitic-charnockitic rocks (Pedrosa-

* Corresponding author.
E-mail address: gelson.ferreira@iag.usp.br (G.F. Souza Junior).

https://doi.org/10.1016/j.tecto.2021.229146
Received 7 May 2021; Received in revised form 3 November 2021; Accepted 8 November 2021
Available online 15 November 2021

Soares et al., 2011; Serrano et al., 2018). The Santa Angélica intrusive complex (SAIC) is one of the post-collisional plutons located in the southern portion of the Araçuaí Orogen (AO). It consists of an oval shaped NE-SW intrusion with an exposure area of 200 km^2 (Wiedemann et al., 2002). It corresponds to two coupled plutons with concentric structures arrayed about a twin, bull's eye pattern decoupled of the regional tectonic features, as indicated by its magnetic fabric (Temporim et al., 2020a). The same authors also described some features, not yet reported in other post-collisional bodies of the AO, such as an intense solid-state deformation at its borders and internal shear zones. The mechanisms responsible to generate such intense deformation in this post-collisional tectonic context remains an unsolved question.

The internal structures and shape of plutons can be used to infer their emplacement mechanisms and the control of the local crustal rheology. Flat-floored bodies are usually related to magma spreading horizontally within a layered crust, commonly occurring in late orogenic environments or extension propagation. Such spreading generates shallow plunging lines consistent with the horizontal elongation direction of the magma body (Vigneresse et al., 1999). On the other hand, wedge-shaped plutons are inferred to fill structures, usually showing sub-vertical walls and being associated with the formation of steeply dipping shear zones. The transition in such behavior is assumed to occur close to the brittle/ductile transition, where the lineation change from low-inclination to steep dip along vertical magma feeding zones (Vigneresse, 1995). When the internal features in the pluton are apparently not superimposed by tectonic structures (Fowler and Paterson, 1997), the foliation and lineation acquired during emplacement show a concentric pattern ("onion skin"), that can be used to define the magmatic feeding zones (Bouchez, 1997; Bouchez et al., 1990). Another common pattern usually occurs in elongated plutons, where the magmatic structures are formed parallel to the elongation of the intrusion and/or of the regional structural tendency (Paterson et al., 1998).

Among all the geophysical observations applied to designate the geometry in depth of intrusive bodies, the gravity method is the most appropriate one, especially when combined with structural data (Améglio and Vigneresse, 1999). This combination of both gravity and structural data (using anisotropy of magnetic susceptibility, AMS) allows one to infer the geometry and structural trend of the last movements of the magma before crystallization is complete, also reflecting the deformation caused in the surrounding crust (Vigneresse et al., 1999).

This paper aims to give a new perspective of the mechanisms responsible for the emplacement of post-collisional plutons and the deformation caused by this process in its country rocks through the example of the SAIC. To achieve that, we modelled the intrusion's shape using gravity methods and used AMS as a structural tool together with detailed microstructural analysis.

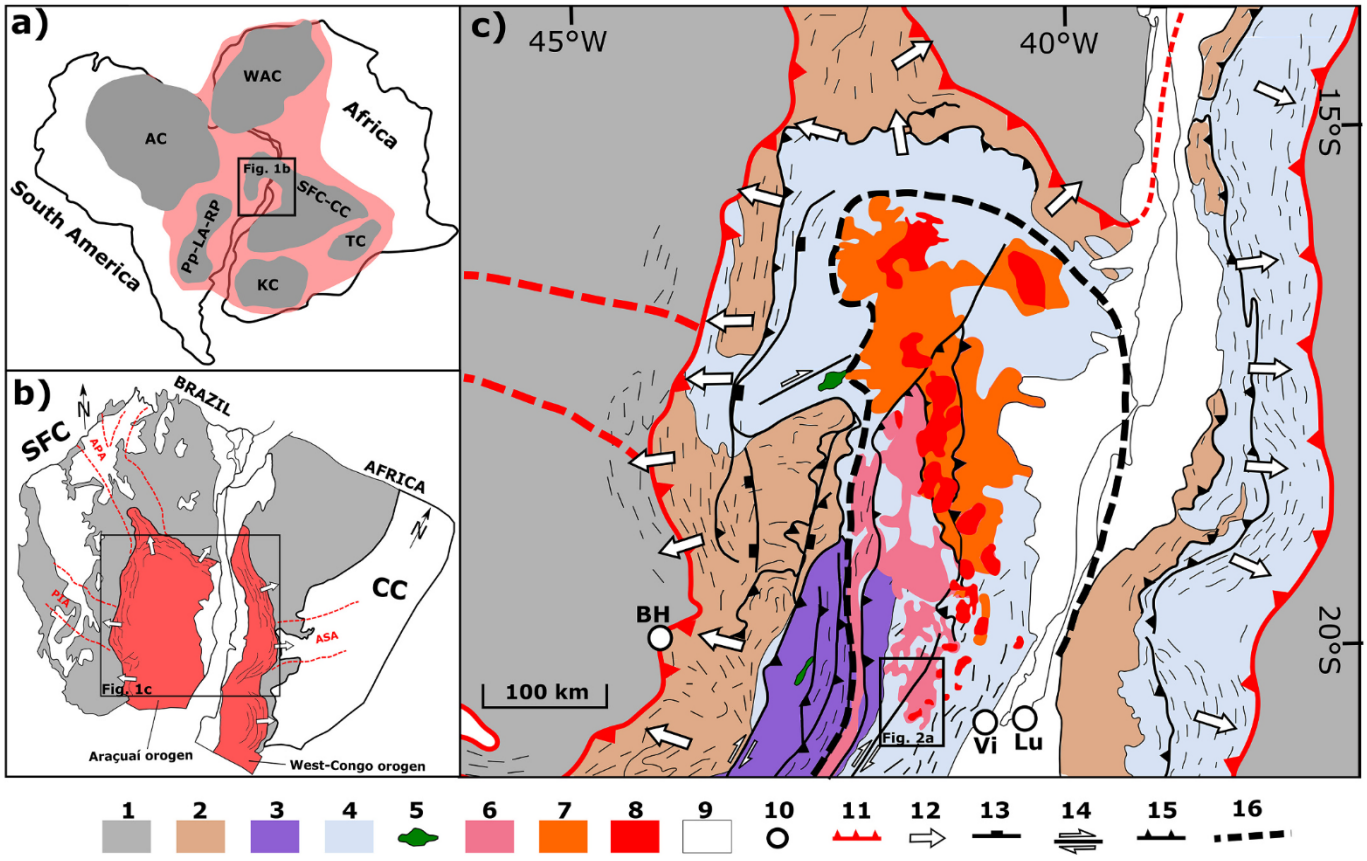

Fig. 1. Regional geological setting of the Araçuaí orogen. (a) Geographical reconstruction of the assembled Western Gondwana by the collision of the following cratons: AC – Amazonian; WAC – West African; TC – Tanzanian; KC – Kalahari; Pp-LA-RP – Paranapanema, Luis Alves and Rio de la Plata; SFC – São Francisco; and CC – Congo (Modified from Alkmim et al., 2006). (b) Emphasis on the tectonic setting and vergence of the Araçuaí-West Congo orogen (AWCO) between the SFC and CC (after Alkmim et al., 2006), also showing the main aulacogens: PIA – Pirapora; APA – Paramirim; and ASA - Sangha. (c) Simplified geological map of the AWCO (modified from Da Silva et al., 2005), the square delimits the study area of the Santa Angélica intrusive complex represented in Fig. 2. Geological and structural units: 1 – cratons; 2 – remobilized basement (Archean - Proterozoic); 3 - allochthonous terrane; 4 – metasedimentary rocks (1.0–0.6 Ga); 5 – ophiolite; 6 – pre-collisional magmatism (G1 supersuite), 7 – syn-orogenic magmatism (G2 and G3 supersuites); 8 – post-collisional magmatism (G4 and G5 supersuites); 9 - Phanerozoic sediments; 10 – cities (Vi – Vitória, Lu – Luanda, and BH – Belo Horizonte), 11 – cratonic limits; 12 – tectonic vergence; 13 – normal faults/shear zones; 14 – transcurrent dextral shear zones; 15 – reverse faults/shear zones; and 16 – AO's crystalline core limit (Alkmim et al., 2006), also coincidently with high temperature hinterland (hot orogenic core) boundary (Fossen et al., 2017).

2. Geological setting

2.1. Regional context

The Araçuaí orogen (AO), together with its counterpart the West-Congo orogen, represents a thrusting belt built through the collision between São Francisco and Congo cratons (Fig. 1a). The collision happened during the Brazilian event, resulted in the amalgamation of the West Gondwana paleocontinent (Alkmim et al., 2006). The orogen evolution is marked by folding and thrusting verging towards the cratonic regions (Fig. 1b), with structural trend parallel to ~N-S. This structure followed a transcurrent, NE-SW with dextral kinematic, deformation in ductile and ductile-brittle conditions and finally a gravitational collapse. The AO's tectonic evolutionary stages is grouped, with different periods of magma production from early Ediacaran to Cambrian (De Campos et al., 2016; Pedrosa-Soares et al., 2011; Wiedemann-Leonardos et al., 2000), in: (i) pre-collisional (630–580 Ma) with the development of an accretionary orogeny marked by the calc-alkaline I-type G1 supersuite; (ii) *syn*-collisional (585–545 Ma) when the main collisional orogeny stage established with the metamorphic peak alongside with partial melting of sedimentary rocks producing the, S-type, G2 supersuite; (iii) late-collisional (545–530 Ma) related to lateral escape with consequent formation of large shear zones and the G3 supersuite; and (iv) post-collisional (530–480 Ma) when the gravitational driven collapse culminated in the production of the G4 and G5 supersuites. Recently, discussions were raised regarding the thermal structure and evolution of the orogen (e.g., Fossen et al., 2020). The Araçuaí-West Congo orogen has also been interpreted as a Neoproterozoic example of hot and intracontinental orogen with little, or no creation of oceanic crust (Cavalcante et al., 2018; Fossen et al., 2017, 2020). This interpretation assumes that volumetrically extensive magmatism occurred for a long period of time associated to a slow cooling rate of 3–5 °C/Ma until 500 Ma, sustaining high geothermal gradients for a long time (Munhá et al., 2005; Petitgirard et al., 2009; Vauchez et al., 2007, 2019).

We focus here on the post-collisional stage. The post-collisional magmatism has been widely studied, especially the G5 supersuite which includes I-Type to A-type, calc-alkaline Fe and K rich granite and its opx-bearing charnockitic analogous (Araujo et al., 2020; De Campos et al., 2004, 2016; Mendes and de Campos, 2012; Serrano et al., 2018; Wiedemann et al., 2002). In the southern portion of the AO, this supersuite is represented by small balloon-like inversely zoned plutons, mainly composed of granitic-charnockitic rocks at the borders and gabbronoritic rocks in the cores, with extensive magma mixing and mingling features between them (De Campos et al., 2004, 2016). However, the northern of the AO outcrops a shallower portion of the crust, where the G5 supersuite exposes much bigger batholiths intrusions (Fig. 1c) constituted of granitic-charnockitic rocks (Pedrosa-Soares et al., 2011; Serrano et al., 2018). The study area is located in the south of AO, containing the Santa Angélica intrusive complex outcropping in the vicinity of Guaçuí shear zone (GSZ), an expressive tardi-collisional feature that imparts important structural control in pre to *syn*-kinematic rocks of AO (Silva, 2010).

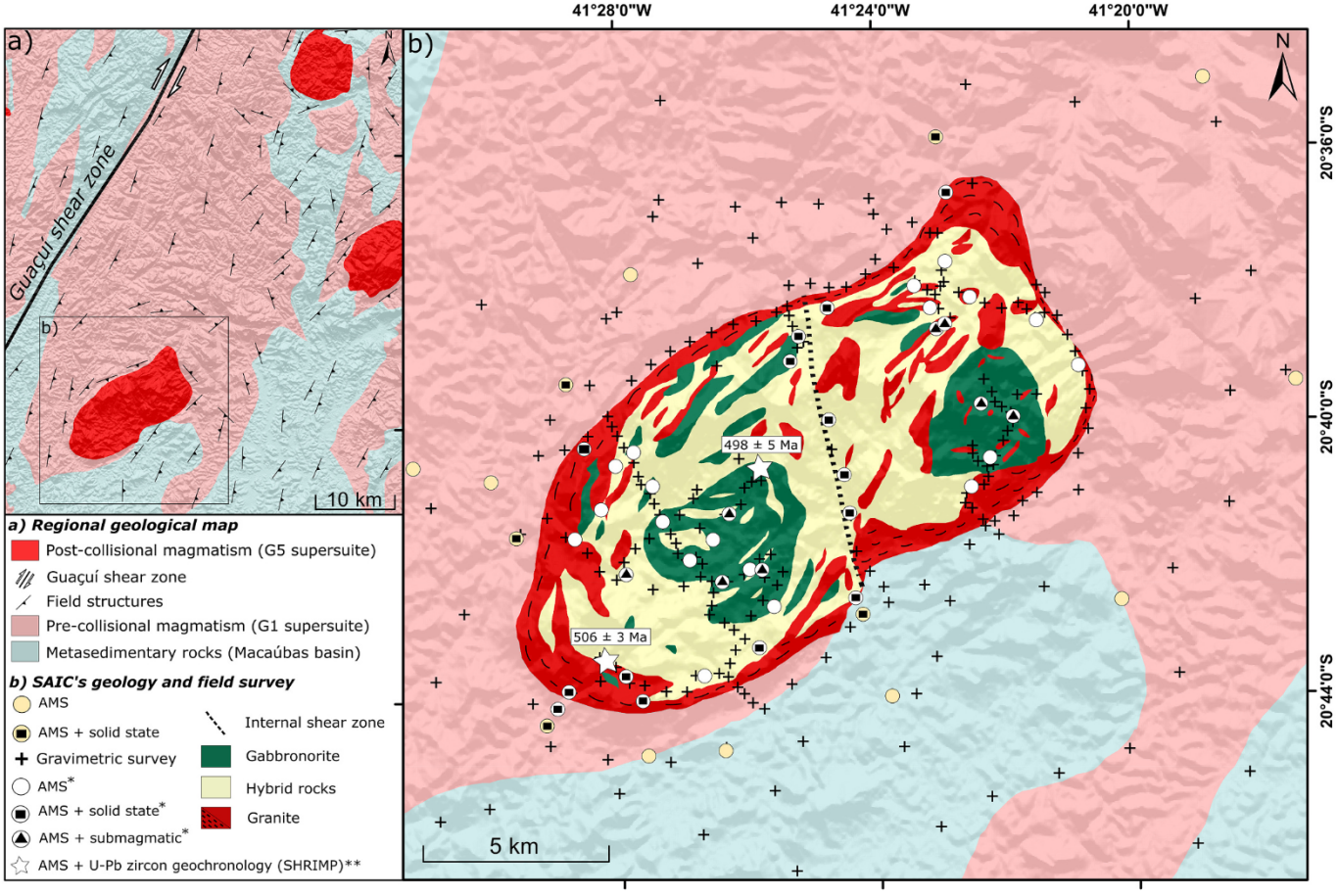

Fig. 2. (a) Simplified geological context within the AO's crystalline core, modified from Pedrosa-Soares and Wiedemann-Leonardos (2000). (b) SAIC geological map (modified from: Schmidt-Thomé and Weber-Diefenbach, 1987); including our gravity stations (+) and sampling sites for AMS measurements complemented with the AMS data, thin-section analysis and geochronology extracted from Temporim et al. (2020a, 2020b) represented in the legend by * and **, respectively.

2.2. The Santa Angélica intrusive complex

The Santa Angélica intrusive complex (SAIC) has an elliptical elongated shape following a northeast axis (Fig. 2) and an exposed area of approximately 200 km^2 (De Campos et al., 2004). The country rocks are high-grade metamorphic, mainly orthogneisses composed of biotite-hornblend-titanite granodiorites to tonalites (G1 supersuite), whereas the minority of paragneisses are composed of biotite-garnet-sillimanite and/or cordierite. The country rocks close to the border have steep foliation (Fig. 3a) and surrounds the pluton as a sheared envelope (Figs. 2a and 3b) that plunges towards the intrusion, whence a mechanism of intrusion by diapirism is proposed (Bayer et al., 1987). At distances greater than 1–2 km from this contact, the foliation assumes an N-S trend typical of the entire Araçuaí orogen (Bayer et al., 1987), or follows the NE-SW trend in the zone under the influence of GSZ (Fig. 2a). This shear zone is defined by vertical to subvertical mylonitic foliation formed under dextral transpressive deformation (Alkmim et al., 2006, 2007; Pedrosa-Soares et al., 2008; Wiedemann-Leonardos et al., 2000).

The SAIC is a representative example of the G5 supersuite, located in the Southern portion of the AO. Its inversely-zoned features with more felsic rocks located in its borders displays well-marked vertical foliation (Fig. 3c) and mafic rocks occurring in their cores (Fig. 2b). The transition between these two regions has an extensive mixing zone with an intermediate composition (Fig. 3d-f) (Bayer et al., 1987; Schmidt-Thomé and Weber-Diefenbach, 1987). In the SAIC core outcrops biotite-monzogabbros and quartz-monzodiorites (498 ± 5 Ma, zircon U—Pb, SHRIMP, Temporim et al., 2020a) with porphyritic texture and oriented phenocrystals (which indicates magmatic flow). In the outermost granitic portion (506 ± 3 Ma, zircon U—Pb, SHRIMP, Temporim et al., 2020a), predominates monzogranites with medium to coarse granulation, of porphyritic texture and accessory phases, such as allanite and titanite (Bayer et al., 1987).

The SAIC has been interpreted as a bull's eyes pattern, with concentric structures arrayed about twin-lobes (Temporim et al., 2020a). The southwest and northeast lobes are separated by an NNW-SSE internal shear zone with evidence of solid-state deformation (Fig. 2b). The granite is highly foliated parallel to the contact with the country rocks in most of SAIC's borders, as well as sub-vertically with clear evidence of solid-state deformation. However, the two lobes have differences between themselves. In the southwest lobe, the magnetic sub-horizontal lineation plunges into the central part of the intrusion and gradually verticalizes towards the borders. In the northeast lobe, the magnetic lineations tend entirely to a vertical plunge. Such contrast is interpreted as outcrops of different intrusion levels, meaning that the southwest lobe exposes the shallowest portion and the northeast one exposes a deeper portion close to the pluton root (Temporim et al., 2020a).

3. Magnetic analyses

3.1. Methods

All measurements were performed at the Laboratório de Paleomagnetismo e Magnetismo de Rochas (USPmag) of the Instituto de Astronomia, Geofísica e Ciências Atmosféricas of the Universidade de São Paulo (IAG-USP). The magnetic susceptibility k describes the quantity of magnetization M that a material acquires when a field H is applied ($M = k^*H$), whereas in a low magnetic field the anisotropy can be geometrically represented as a triaxial ellipsoid (k_1, k_2, and k_3) featuring a second-rank tensor (Collinson, 1983). The anisotropy of magnetic susceptibility (AMS) technique was applied to investigate the main directions of magnetic foliation (k_1-k_2, the plane orthogonal to k_3) and magnetic lineation (k_1) present in the SAIC's country rocks. For such purpose, drilled cores were sampled at 15 sites around the SAIC with

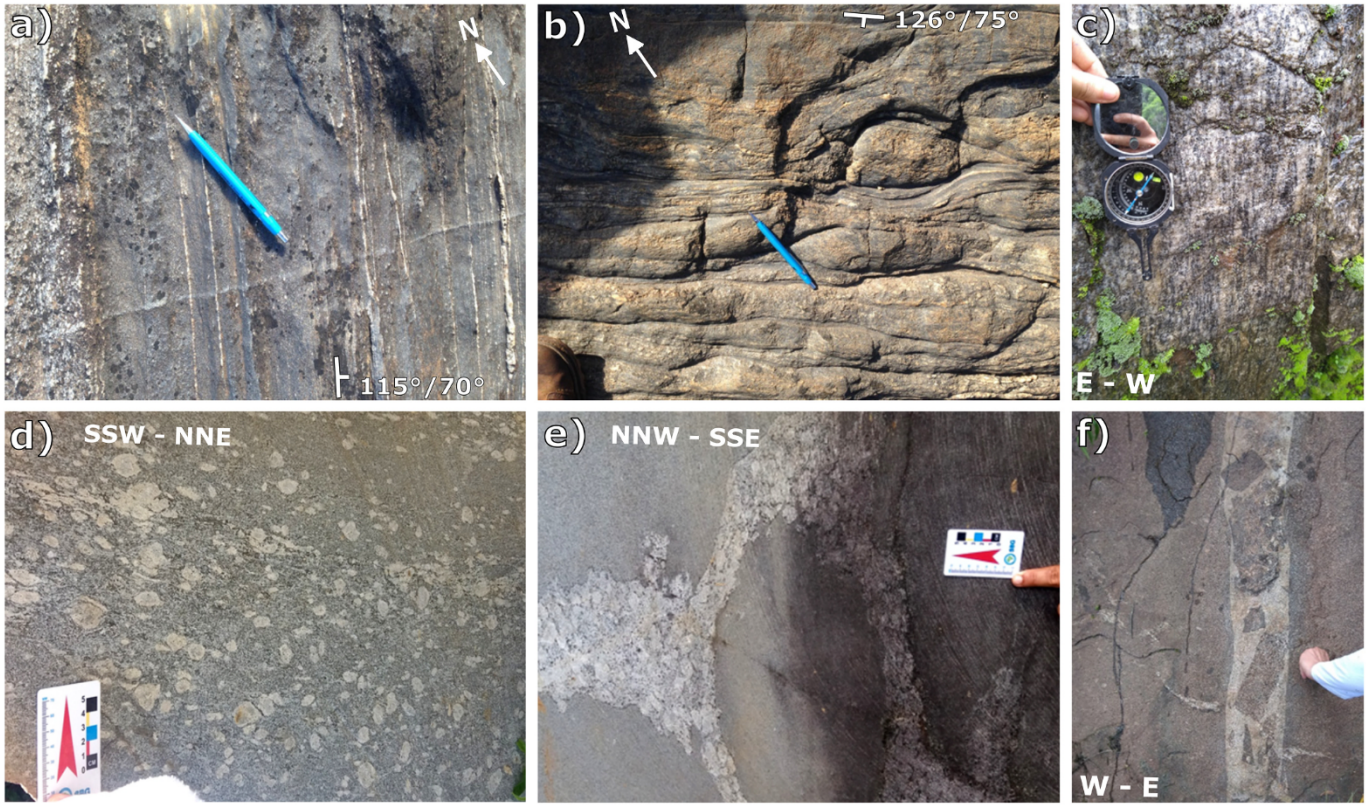

Fig. 3. (a) Country rock orthogneiss showing strong steep foliation; (b) shear structures with the same direction as the contact and dextral kinematics in the country rocks near the SAIC border; (c) sheared granite in SAIC borders; mixing zone rocks with (d) low viscosity and almost homogenous mixture; (e) medium viscosity producing inhomogeneous mixtures; and (f) high viscosity with no mixing, generating sharp enclaves.

different distances from the contact, extracted with the aid of a portable gasoline drill fitted with a diamond-tipped water-cooled bit. At least 8 cores were extracted at each site with an approximate length of 15 cm and 2.5 cm in diameter. Samples were subsequently sawed into 2.2 cm long cylindrical discs, thus generating a total of 163 specimens for magnetic analysis and to calculate the bulk density of the rocks. AMS at a low field was measured using the Kappabridge MFK1-FA Multi-Function equipment (AGICO, 300 A/m and alternating field at 970 Hz) and the data were processed using the Anisoft5 software (AGICO). Average directions of the three main axes of ASM were obtained, as well as other anisotropic parameters, such as K_m (bulk magnetic susceptibility), P (anisotropy degree), T (shape), and the internal dispersion for each AMS axis (ε_{12}, ε_{23}, ε_{31}), following Jelínek (1978).

Complementing the country rock's AMS measurements, the anhysteretic anisotropy of remanent magnetization (AARM) method was applied at 4 sites (SAG1, SAG3, SAG8, and SAG12–6 specimens per site) to investigate the sole ferromagnetic (*lato* sensu) contribution in the mineral fabric, because paramagnetic and diamagnetic minerals are incapable of retaining a remanent magnetization, as proposed by Jackson (1991). The samples were demagnetized in an alternating field of 100 mT, using the equipment LDA-3 (AGICO) decreasing to zero over a period of one minute. Subsequently, the samples were imparted with anhysteretic remanences at an AF peak field of 50 mT (direct field of the 500 μT), a value chosen after an analysis of the remanent magnetization spectrum, following a 12 positions protocol. Thus, the remanent magnetization of each position was obtained using a JR-6 spinner magnetometer through Rema6 (AGICO) software. Processing was performed, also using the software Anisoft5, to obtain the average directions of the three remanent magnetization axes. Similar to the AMS, the AARM data can be geometrically represented as a triaxial ellipsoid (M_1, M_2, and M_3). To investigate the contributions of high and low coercivity signatures in the country rocks, samples from SAG1 and SAG12 sites were submitted to additional steps of AARM acquisition. Partial AARM procedures followed Trindade et al. (2001), and consisted in the magnetization of 12 samples in a direct field of the 500 μT while affected by the alternating field of 100 mT, followed by demagnetization

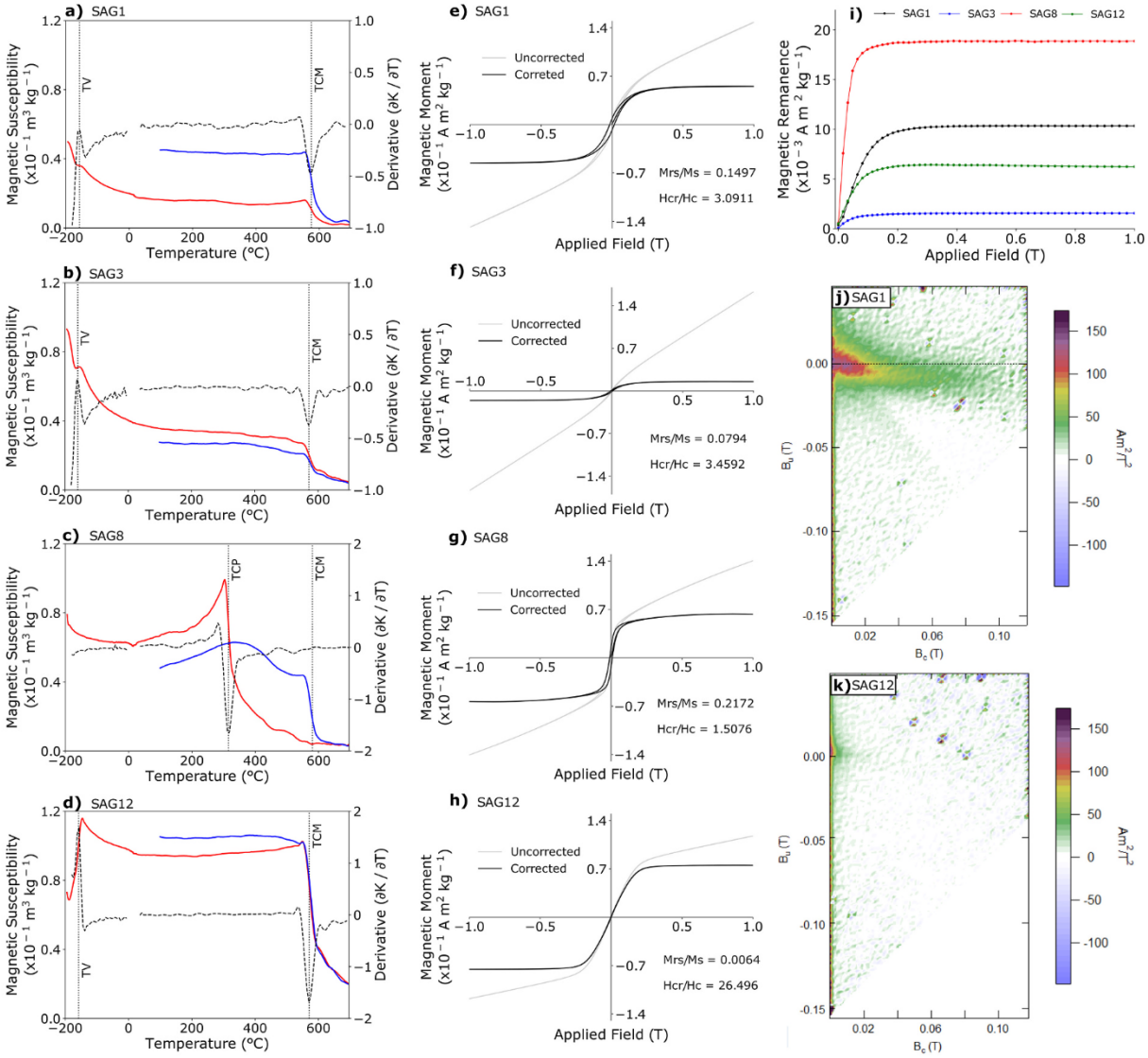

Fig. 4. Representative magnetic mineralogical analyses of the country rocks. Thermomagnetic curves (a-d), the y-axis is the bulk of magnetic susceptibility normalized by the bulk density and the x-axis is the temperature in degrees Celsius. The red lines represent the heating cycle, blue lines represent the cooling cycle, the black dashed lines are the first derivative ($\partial k/\partial T$), TV = Verwey transition, TCM = magnetite Curie temperature and TCP = pyrrhotite Curie temperature. Hysteresis curves (e-h) and IRM acquisition (i) for the same sites, the magnetic moment was normalized by the mass. The FORC diagrams applied for the one site near the contact with the SAIC (j) and one relatively far from the latter (k). (For interpretation of the references to colour in this figure legend, the reader is referred to the web version of this article.)

in an alternated field of 70 mT in each position, therefore, it was possible to extract two partial directions.

To investigate the country rocks magnetic mineralogy, thermomagnetic experiments were carried out on the same four sites where AARM was applied. To accomplish that, the samples were crushed into a powder using an agate mortar then measurements were acquired using the Agico Kappabride KLY 4 CS, in both low and high-temperature cycles. The low-temperature cycle was executed with the CSL cryostat apparatus, applying liquid nitrogen until the sample reached −192 °C. Magnetic susceptibility vs temperature data was, automatically and continually, measured during this cycle as the sample spontaneously reached room temperature (20 °C). Using the same samples, the high-temperature cycle was conducted with CS4 furnace apparatus by heating them from the room temperature until around 710 °C and then cooled until 100 °C. During the whole process, the magnetic susceptibility vs temperature data were acquired, such as in the low-temperature cycle. Through the high-temperature cycle, samples were under an argon atmosphere to avoid excessive oxidation/mineral transformation. To define more precisely the main magnetic transitions, the first derivative ($\partial k/\partial T$) was applied in the heating curves through the finite difference method. To complete the magnetic mineralogy investigation, isothermal remanent magnetization (IRM) curves, magnetic hysteresis and first-order reversal curves (FORCs) were acquired using a MicroMag 3900 vibrating sample magnetometer (VSM) to investigate the domain state.

3.2. Magnetic mineralogy of country rocks

The k-T curves with the lowest magnetic susceptibility (Fig. 4a, b) show similar responses, during both heating (−192 °C – 710 °C, the red lines) and cooling cycles (710 °C – 100 °C, the blue lines). Such is a paramagnetic behavior with poorly defined transition at temperatures around −157 °C (more visible in the derivative curves, the dashed black line) and drops above 580 °C, which are coincident with the Verwey transition and the Curie temperature for the magnetite ($Fe_{3-x}Ti_xO_4$, $x \cong 0$), respectively (Dunlop and Özdemir, 1997), indicating some contribution of the latter in the mineral fabric. The k-T graph shown in the Fig. 4c reveals a steep magnetic susceptibility drop around 320 °C in the heating curve, and a raise in the magnetic susceptibility at the temperature of 580 °C during the cooling cycle. We interpreted it as an indication of pyrrhotite grains, which are then converted to magnetite during the heating cycle. Fig. 4d shows a classic thermomagnetic curve of magnetite with both transitions at temperatures of −153 °C and 580 °C well defined.

The hysteresis loops (Fig. 4e-h) and IRM (Fig. 4i) applied to investigate the country rock magnetic domain states show an interesting relation between sheared rocks and coercivity. The sites with field evidence of shear deformation, e.g., SAG1 (Fig. 3b) and SAG8, reflect hysteresis loops with higher coercivity and classified as pseudo single domain (PSD), once the ratios of Mrs./Ms. and Hcr/Hc fall in PSD spectrum in the Dayplot (Day et al., 1977). Such behavior is also confirmed by the FORC diagram (Fig. 4j), as proposed by Roberts et al. (2000). While, the sites without of shear deformation (e.g., SAG3 and SAG12) show thin hysteresis loops (i.e., lower coercivity) and classified as multi domain (MD), also confirmed by the qualitative analysis in the FORC diagram that shows wide spreading in the interaction axis (*Bu*) and low coercivity (*Bc*) (Fig. 4k) (Roberts et al., 2000).

3.3. Previous results on the internal structure of the Santa Angelica intrusion

Constricted magnetic hysteresis and first-order reversal curves alongside with thermomagnetic curves indicate low-coercivity multi-domain magnetite as the main carrier of the magnetic fabric in all facies of the SAIC (Temporim et al., 2020a). The AMS and AARM magnetic fabric are very similar for all lithotypes, attesting the dominant role of the multi-domain magnetite in the definition of the magnetic fabric in these rocks. This indicates that the dispersion in the AMS fabric of these sites is not related to the influence of other magnetic phases, but mainly reflects the dispersion in the orientation of the MD magnetite grains in the rock (Temporim et al., 2020a).

The AMS data (Temporim et al., 2020b) also indicate that the emplacement of the intrusive complex corresponds to twin plutons with concentric structures (Fig. 5a) arrayed about bull's eyes pattern (Temporim et al., 2020a). The macroscopic foliation recognized closer to the contact boundaries is observed as a magnetic foliation that contours the pluton boundaries. This foliation dips steeply, and magnetic lineations are also steeply plunging (Fig. 5b). The southwest lobe presents magnetic lineations varying from low to high angles (Fig. 5c), the lowest angles occur near the mafic core. In all petrographic facies, the northeast lobe presents near-vertical magnetic lineations and foliations (Fig. 5d). The internal shear zone geometry is well resolved by parallel AMS fabrics at all sites along the NNW-SSE oriented structure. Magnetic foliation strikes NNW-SSE with steep dips, and magnetic lineations have high rakes, consistent with the NE vergence (Fig. 5e).

3.4. New results on the magnetic anisotropy of the country rocks

The data of the sites sampled in the country rock are shown in the Table 1. The bulk magnetic susceptibility (K_m in SI units) values range from 0.1029×10^{-3} to 11.1×10^{-3}. At least half of the sites have $K_m < 0.5 \times 10^{-3}$, which according to Rochette (1987) might be a paramagnetic rock behavior caused by iron-bearing silicates such as biotite and amphibole. The K_m in the country rocks is usually two orders of magnitude smaller than the ones measured in the SAIC rocks (Temporim et al., 2020a). The anisotropy parameter (P), used to measure the magnetic anisotropy degree in the samples (Nagata, 1961), values vary between 1.044 and 1.435. As stated by Bouchez (1997) values of $P \leq 1.15$ corresponds to paramagnetic granitic rocks with biotite and magnetite in their mineral fabric. This statement is coherent with the SAIC's country rocks data, since the samples with $P > 1.15$ (e.g., SAG1, SAG3 and SAG12) have biotite and opaques (magnetite confirmed in the thermomagnetic curves) in their mineral fabrics, while the sample with $P < 1.15$ (SAG8) has biotite and pyrrhotite (also confirmed in the thermomagnetic curves). The shape parameter (T) was used to characterize the ASM ellipsoids of the magnetic fabric (Hrouda, 1982), in which: (i) negative values indicate a prolate shape and (ii) positive values reveal an oblate shape. Although T values of SAIC's country rocks varied from −0.118 to 0.655, the majority of their mean values are positive (Table 1). Therefore, represents an oblate fabric coherent with the metamorphic foliation and the deformation imparted on them.

In the country rock's AMS data, there is a duality in behavior: (i) near the contact with the SAIC, both magnetic foliation and lineation (Fig. 5a, f) tend to verticalize, similar to what Temporim et al. (2020a) describe to occur with the border granite, diving towards the contact direction; and (ii) when moving away from that contact, the AMS and field directions assume the regional trend (AO or GSZ). Nevertheless, even at greater distances (i.e., >4 km) from the contact, there are still deflections in the magnetic foliation caused by the deformation associated with the SAIC emplacement process.

The Fig. 6 shows the AMS and AARM results for the country rocks. The AMS and AARM magnetic fabric are coincident for all specimens with remanent magnetization response measured between 0 and 50 mT, therefore attesting the dominant role of the MD, mainly magnetite, in the definition of the magnetic fabric in these rocks. Petrographic studies reveal elongated anhedral opaque minerals with preferred crystal orientation parallel to the orientation of biotite, amphibole and feldspars. The high coercivity (70–100 mT) AARM response is also similar to the AMS for the site SAG01, while the site SAG12 shows a random distribution of directions. As already mentioned, FORC diagrams shows that SAG01 has a PSD signature (Fig. 4j), while the SAG12 magnetic carriers are MD (Fig. 4k). Consequently, the contribution of MD particles

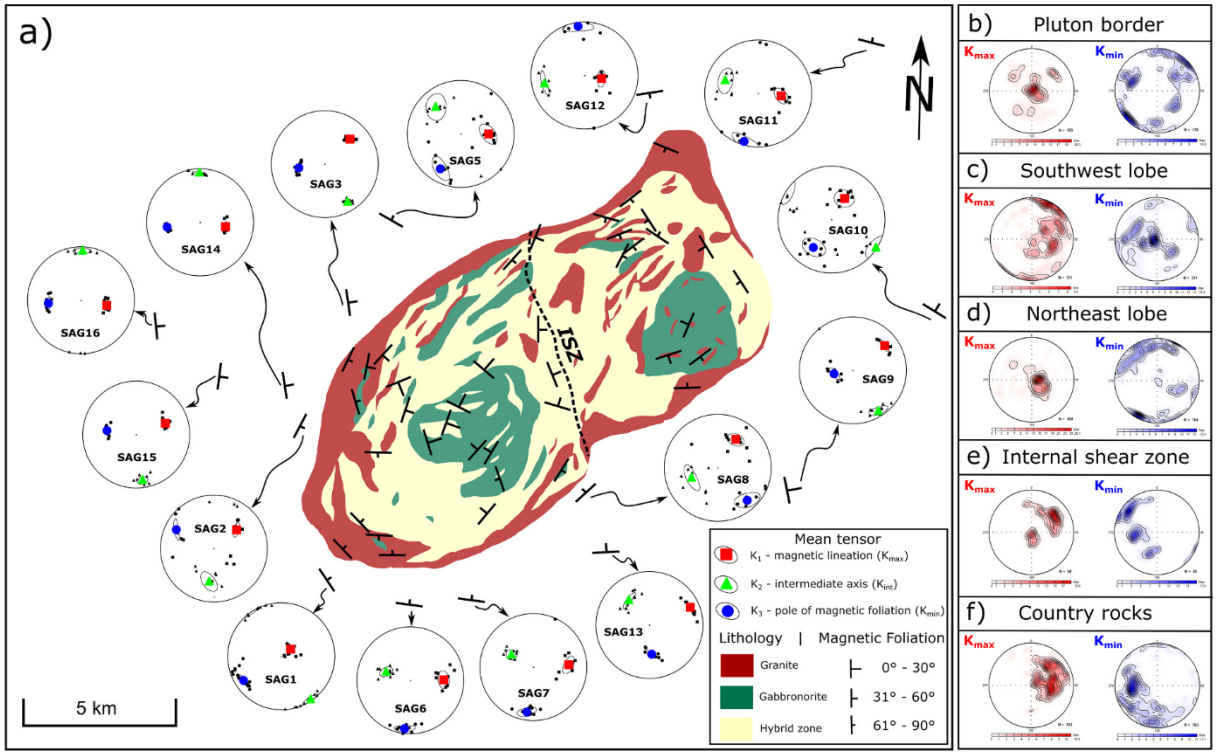

Fig. 5. (a) Anisotropy of Magnetic Susceptibility results for each sampling site in the SAIC (data from Temporim et al., 2020b) and its country rocks (this work), ISZ = internal shear zone. The distribution of the magnetic lineations (K_{max}) and pole of magnetic foliations (K_{min}), respectively, for (b) granitic border, (c) southwest lobe, (d) northeast lobe, (e) internal shear zone and (f) country rocks. Averages were determined for 7–10 measurements per site.

Table 1
Anisotropy of magnetic susceptibility average parameters for the SAIC's country rocks.

Site	N	Geographic coordinates		Scalar data			AMS axes directions					
		Longitude (W)	Latitude (S)	K_m (10^{-3}SI)	P	T	K_1	ε_{12} (K_1)	K_2	ε_{23} (K_2)	K_3	ε_{31} (K_3)
SAG01[a]	18	41° 29′ 10.032″	20° 44′ 20.975″	10.52	1.435	0.007	49.1/72.2	6.3/4.4	145.9/2.2	10.1/5.9	236.6/17.6	10.1/3.9
SAG02[a]	11	41° 29′ 35.849″	20° 41′ 36.640″	0.1029	1.181	0.547	50.0/44.7	11.7/3.9	189.0/37.4	17.5/9.3	296.7/21.8	16.2/3.5
SAG03[a]	8	41° 28′ 47.726″	20° 39′ 22.563″	1.409	1.206	0.055	45.2/34.3	8.7/2.9	148.8/19.0	6.1/4.1	262.5/49.4	9.6/3.6
SAG05[a]	10	41° 27′ 46.096″	20° 37′ 47.193″	4.178	1.460	−0.092	89.4/47.4	17.4/10.2	317.5/31.6	21.7/14.4	210.5/25.4	19.8/9.9
SAG06[b]	10	41° 27′ 35.763″	20° 44′ 48.565″	0.9763	1.315	0.448	88.6/37.8	12.5/9.4	289.6/50.3	10.6/6.6	186.8/10.4	12.7/6.0
SAG07[b]	10	41° 26′ 23.895″	20° 44′ 44.973″	0.1896	1.143	0.155	86.4/34.6	13.9/7.5	299.3/50.6	8.8/7.1	188.2/16.5	13.3/7.4
SAG08[b]	10	41° 24′ 14.482″	20° 42′ 47.169″	0.3806	1.044	0.099	32.0/37.7	12.3/9.6	249.0/46.0	20.1/8.4	137.7/19.3	19.0/11.1
SAG09[a]	10	41° 20′ 13.710″	20° 42′ 36.897″	0.1678	1.144	0.505	51.9/25.9	9.5/3.9	147.8/11.9	12.5/6.7	260.2/61.1	10.9/4.2
SAG10[a]	11	41° 17′ 29.040″	20° 39′ 26.133″	7.76	1.325	−0.351	30.7/51.9	14.8/13.3	122.1/1.1	17.4/13.7	212.9/38.1	17.0/13.9
SAG11[a]	8	41° 18′ 51.722″	20° 35′ 00.757″	11.1	1.419	−0.118	95.7/54.7	13.5/8.4	291.3/34.3	17.6/12.3	196.2/7.4	17.7/9.5
SAG12[a]	7	41° 23′ 00.674″	20° 35′ 50.463″	2.314	1.307	−0.098	100.0/64.2	12.8/5.9	258.7/24.3	16.9/4.7	352.5/8.3	18.4/9.0
SAG13[a]	10	41° 23′ 48.320″	20° 43′ 59.181″	0.1778	1.166	0.593	66.2/18.7	11.6/1.4	320.0/39.5	13.8/3.9	175.7/44.6	10.4/2.6
SAG14[a]	10	41° 29′ 58.773″	20° 40′ 47.386″	0.3218	1.169	0.655	99.5/50.5	7.8/1.7	359.0/8.6	8.4/1.8	262.1/38.2	4.5/1.5
SAG15[a]	10	41° 31′ 10.956″	20° 40′ 34.340″	0.3242	1.119	0.426	68.5/41.8	6.7/2.9	172.5/15.2	6.8/6.3	277.8/44.3	6.4/2.8
SAG16[a]	10	41° 32′ 21.010″	20° 39′ 40.848″	0.1808	1.183	0.586	101.1/49.9	7.7/2.8	1.4/8.0	10.8/5.2	264.9/38.9	9.2/2.7

Site sampled; number of specimens measured (N); longitude, latitude – geographical coordinates (DMS); K_m = bulk magnetic susceptibility (10^{-3} SI); P = degree of anisotropy of the magnetic susceptibility (P = K_1/K_3); T = AMS ellipsoid shape parameter [$T = 2 * \ln(K_2/K_3) / \ln(K_1/K_3) - 1$]; K_1 = azimuth and plunge of magnetic lineation (in degrees); K_2 = azimuth and plunge of the intermediate anisotropy axis; K_3 = azimuth and plunge of the pole of the magnetic foliation; ε_{12}, ε_{23} and ε_{31} are the semi-angle (in degrees) of confidence ellipses of AMS axes from Jelínek (1978) statistics.

[a] Orthogneisses.

[b] Paragneisses.

of SAG12 does not extend to higher values of the coercivity spectrum investigated through partial AARM, explaining why its distribution is randomized.

4. Microstructures

4.1. Methods

Studying the mineral fabric in plutonic rocks necessarily requires the distinction of magmatic and submagmatic structures from the superimposed solid-state microstructures, therefore, using the criteria presented in several papers (e.g., Blumenfeld and Bouchez, 1988; Paterson et al., 1989; Vernon, 2000). As described by Arzi (1978), the microstructures are dependent on the magma rheology, i.e., magmatic structures occurs when magma does not have sufficient solid particles, less than 60% of its volume, and the melt phase restrains any interaction between crystals, allowing free rotation. The submagmatic structures occurs when the solid fraction increases enough to make the magma to

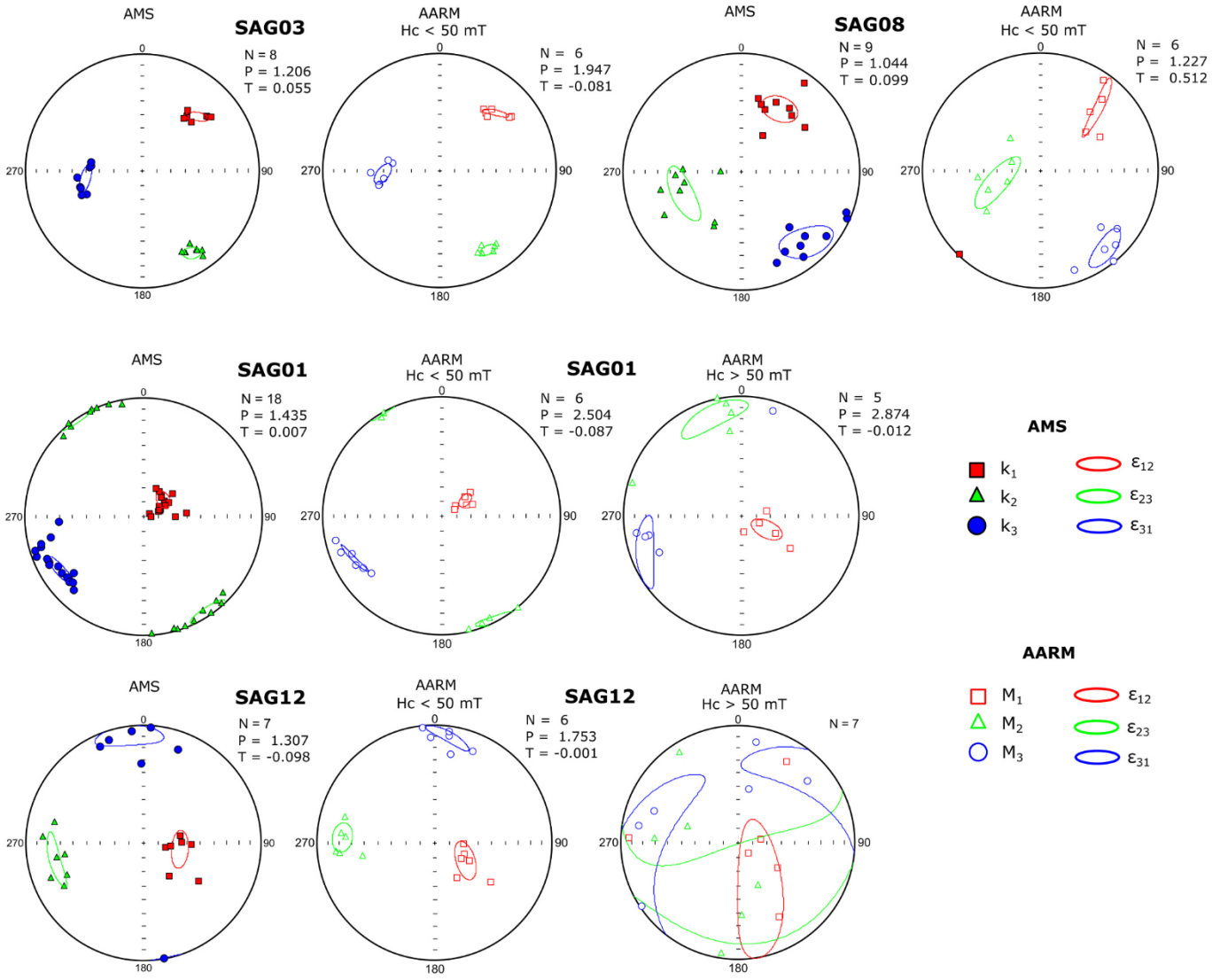

Fig. 6. Comparison of AARM and AMS directions for sites SAG01, SAG03, SAG08, and SAG12. While AMS is the bulk magnetic response of all minerals (dia, para, and ferromagnetic), the AARM isolates the ferromagnetic response and, in this case, is almost exclusively controlled by the shape anisotropy of MD magnetite (SAG01, SAG03 and SAG12) and MD pyrrhotite (SAG08).

behave partially like a solid, whence the amount of melt is insufficient to permit magmatic flow (Bouchez et al., 1992; Paterson et al., 1989). The solid-state deformation that occurs in almost fully crystallized plutonic rocks is more related to metamorphic processes than to the magmatic ones, and can be characterized in mylonitic microstructures range that includes ribbon-quartz, shear bands, fine grained fabric sizes, microstructures produced by dynamic recrystallization (e.g., S/C foliation, undulose extinction, chessboard extinction), and retrograde mineral assemblage (Vernon, 1988, 2000; Vernon et al., 1983).

We assessed the microstructure and kinematics using thin-sections sampled perpendicular to the main foliation (XY plane of the strain ellipsoid formed by the axes) and parallel to the mineral lineation (X). Determining the strain ellipsoid axes is not a straightforward task, especially in cases of plutonic rocks, whence these axes normally have low asymmetry between themselves. The magnetic anisotropy was fundamental to determine igneous fabric for its extreme sensitivity, enabling specifying the strain axes ($X > Y > Z$), as they are, usually, analogous to the axes obtained with the ASM technique ($k_1 > k_2 > k_3$, respectively).

The axis of minimum susceptibility k_3 coincided with the magnetic foliation pole, defined by the plane k_1-k_2 (Archanjo et al., 1995), which is similar to the interpretation of the strain ellipsoid. Ideally, planar and tabular minerals, such as biotite and plagioclase, respectively, define the rock foliation, which coincides with the magnetic foliation. While the magnetic lineation (k_1) matches the crystallographic axis of elongation (c-axis) of prismatic and tabular minerals (Bouchez, 1997).

Twelve thin-section samples parallel to k_1-k_3 plane (same as XZ) were confectioned through the AMS orientation acquired from the cylindrical specimens. Five of them from the SAIC's borders, three sections from the internal shear zone, and the others four from the country rocks near to the contact.

4.2. Microstructural analysis

The country rocks show expressive features of solid-state deformation. However, the deformational halo formed by the emplacement of SAIC, where occurs the deflection of the regional foliation parallel to the contact, shows high temperature microstructures, like ribbon and chessboard undulose textures. These are overwritten by low temperature structures: (i) bulging recrystallization in quartz (Stipp et al., 2002) and (ii) recrystallized chlorite with boudin-like shape (Fig. 7a). SAIC rocks display evidence of submagmatic to solid-state textures, the first

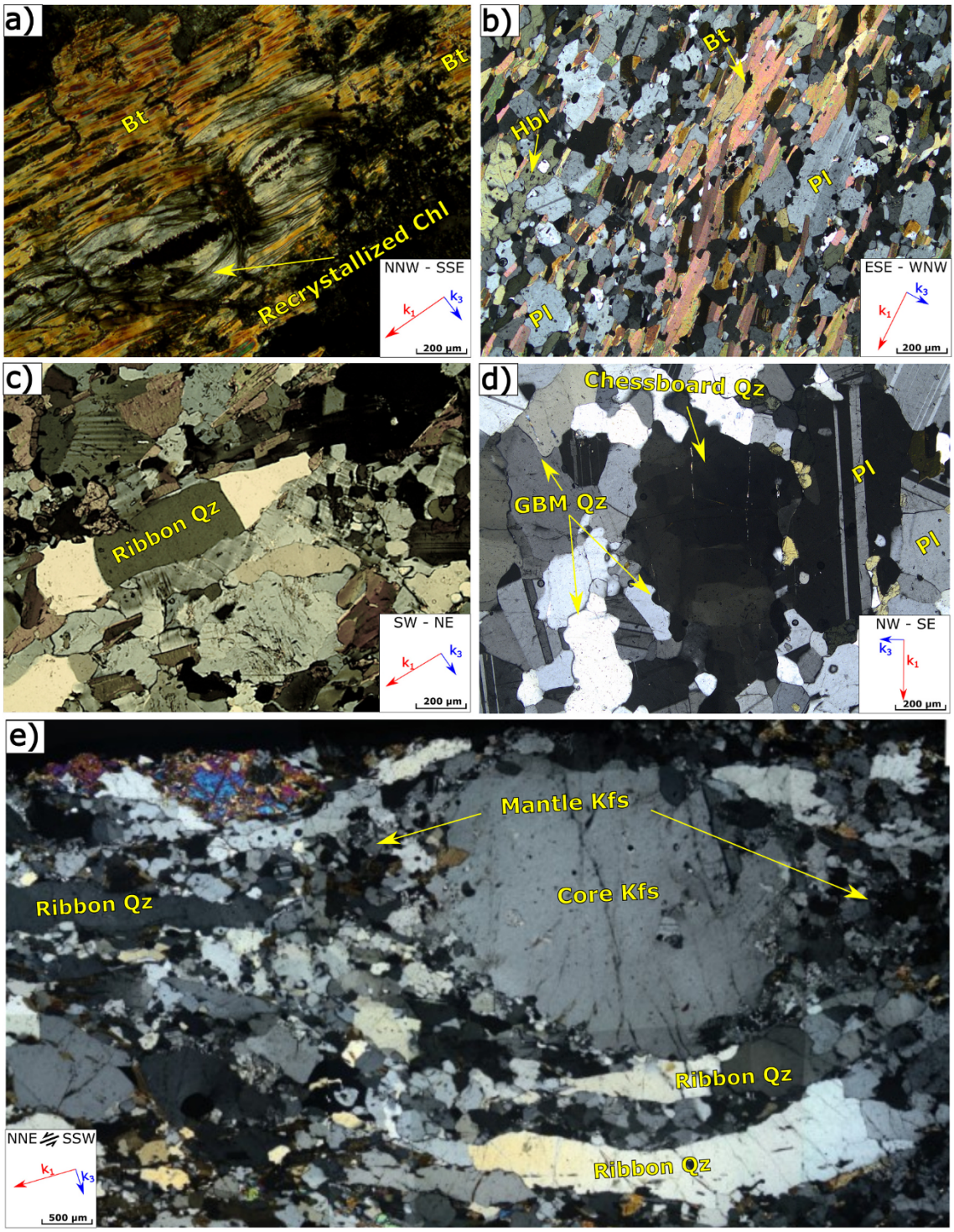

Fig. 7. Images of microstructures of the SAIC and country rocks: (a) country rock thin-section with recrystallized boudin-like chlorite (Chl) parallel to the contact with the SAIC; (b) biotite (Bt) and the Hornblende (Hbl) marking SAIC's granitic border foliation; (c) solid-state ribbon-quartz (Qz) with visible subgrain limits in the granitic border; (d) high-temperature solid-state features of chessboard-like pattern and grain boundary migration, both in grains of quartz in the internal shear zone; (e) high temperature core-and-mantle texture characterized by K-feldspar (Kfs) porphyroclast bordered by well-developed ribbon quartz (showing sinistral kinematics) and undulose felsic aggregates of quartz, K-feldspar and plagioclase (Pl).

one occurring typically in the central parts of the twin lobes (Temporim et al., 2020a). Solid-state microstructures are more common in the borders and in the internal shear zone. The borders usually show a well-marked foliation (Fig. 7b), especially composed of biotite crystals and amphibole (nematolepidoblastic fabric), with a comminution matrix composed by fractured anhedral mafic grains and felsic aggregates. Megacrysts are commonly undulose plagioclase and/or quartz in the form of ribbons (Fig. 7c) and chessboard undulose. The internal shear zone shows only high temperature microstructures, such as: (i) chessboard undulose extinction (Vernon, 2018) (Fig. 7d), (ii) monomineralic ribbon-quartz (Passchier and Trouw, 2005) and (iii) high temperature grain boundary migration (GBM-quartz) (Fig. 7d) (Stipp et al., 2002).

The core-and-mantle plagioclase megacrysts act as porphyroclasts, surrounded by felsic aggregates (Passchier and Trouw, 2005). Well-developed quartz ribbons mark the S foliation (Fig. 7e), which associated with the AMS orientation allowed a kinematic analysis.

5. Gravimetry

5.1. Methods

We used two different gravity datasets in this work. The regional dataset belongs to the Brazilian National Gravity Database (Banco Nacional de Dados Gravimétricos, BNDG) with approximately 400 stations spaced by about 3 km along the main roads. The local dataset was collected during fieldwork in 2019, composing 227 new gravity stations (Fig. 2b). Gravity data was acquired using a Lacoste and Romberg gravimeter, model G, with precision of ±0.01 mGal. The orthometric altitude was measured with a Differential Global Positioning System (DGPS) equipment (± 0.3 m). The gravity data coverage varied from one station each 0.3 km composing three profiles crosscutting the SAIC (Fig. 2b), two transecting each lobe and one along the internal shear zone. Meanwhile, in the country rocks, the coverage was about one station per 4 km to complement the already existing regional gravity dataset. The gravity anomaly, with the drift and tidal corrections applied, was reduced to the 1967 reference ellipsoid and the Bouguer anomaly was obtained after performing the Free-air and Bouguer correction. Chapin (1996) states that the Bouguer plateau density should be chose carefully to avoid mistaken values. Therefore, we calculated the average density of the country rocks using the cylindrical samples, which resulted in $\rho_{Avg} = 2670\ kg/m^3$. The Bouguer anomaly map (Fig. 8) was interpolated using the standard minimum curvature algorithm to generate a regular grid (250 × 250 m).

5.1.1. Gravity field modelling

Additionally regional-residual separation methods were applied in order to highlight the gravity anomaly related to the SAIC rocks: (i) omission of points (Fig. 9a, b); (ii) upward continuation (Fig. 9c, d); and (iii) third order polynomial fit (Fig. 9e, f). To forward modelling, the residual anomaly data was used as the observed gravity, together with three physical constraints: (i) a simplified SAIC geological map with three main facies (mafic cores, hybrid zone and granitic border), (ii) a digital elevation model of SAIC and surrounding areas, and (iii) the calculated average density of the SAIC and its country rocks using the same cylindrical specimens from the magnetic study.

The forward gravity modelling was performed using GM-SYS (Oasis Montaj software) based on 2D formulation (Talwani et al., 1959). The calculated gravity anomaly was compared to the observed, while the volumes of the models were modified until their residue was below 5%. Since only the SAIC gravity anomaly was isolated, the density used

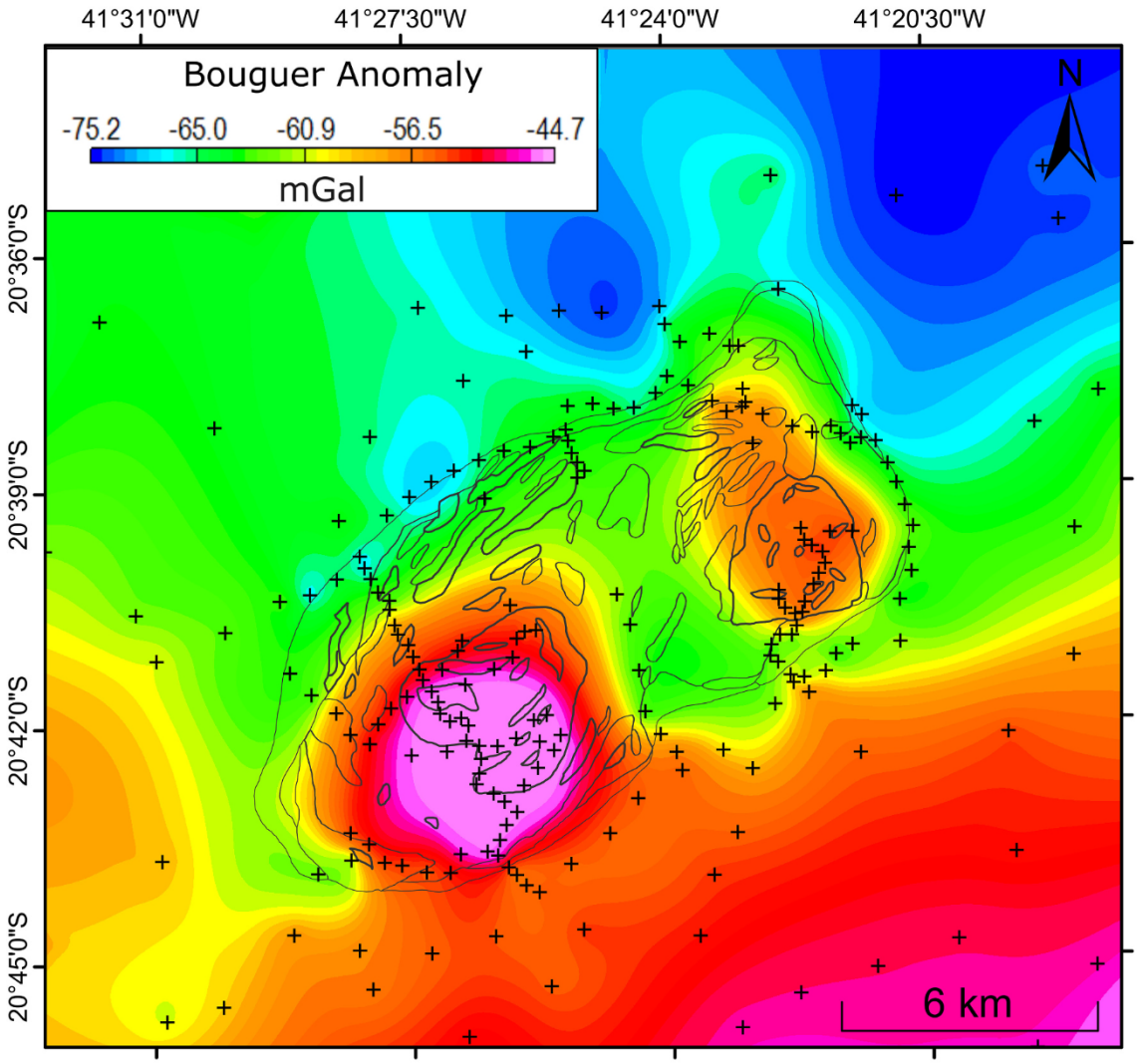

Fig. 8. Bouguer anomaly map, the cross symbol represents the measured gravimetric stations.

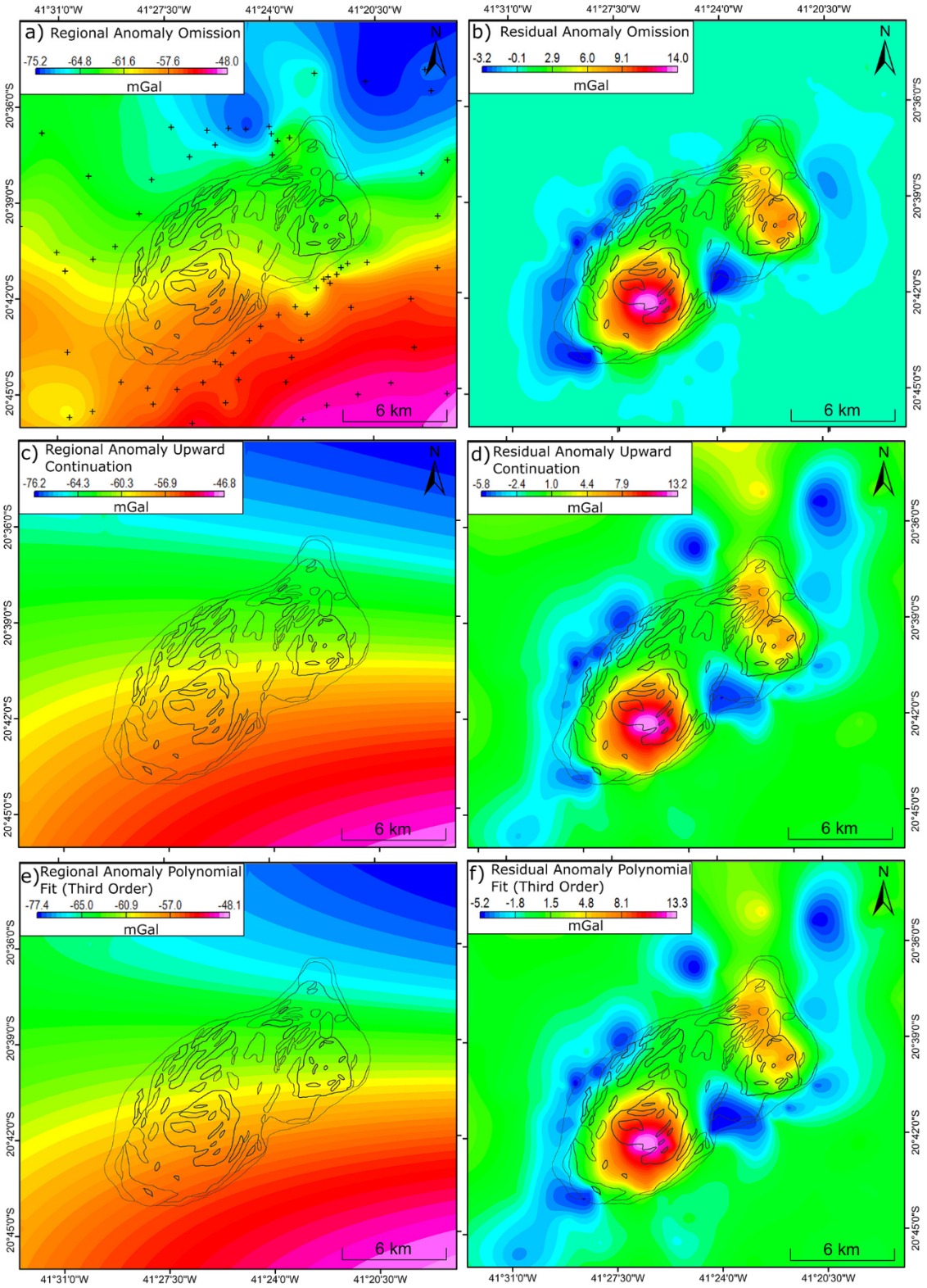

Fig. 9. The comparison of the regional-residual separation techniques performed with the regional and residual anomalies represented respectively: (a and b) the omission of points method, the cross symbol also represents the gravimetric stations kept in the database during the interpolation; (c and d) upward continuation; and (e and f) third order polynomial fit.

during the modelling was calculated subtracting the country rock average density from the SAIC rocks. In order to estimate the pluton's depth more precisely, five profiles were built, three of them transecting obliquely the SAIC and the other ones transecting it longitudinally.

5.2. *Bouguer and residual anomalies*

The Bouguer Anomaly is a result of the lateral density contrast between rocks (Améglio et al., 1997). However, long-wavelength regional anomalies are caused by the effect of deeper density contrasts (Telford

et al., 1990). On the other hand, short-wavelength anomalies, called residual anomalies, are caused by anomalous mass distribution of shallower portions of the crust (Lowrie, 1997). Thus, it is possible to discern a strong contribution of the mafic core of the intrusive complex in the Bouguer data (Fig. 8), but as this product is not ideal for the study of a body with a more restricted area, it was necessary to apply the regional-residual separation method to isolate the effect of the intrusive body.

Although we tested different regional-residual separation methods, we choose the omission of points because it seems to be best one to reflect the geological distribution of the SAIC rocks and also to remove the short-wavelength anomalies related to the country rocks. This method is based on removing the gravity stations within the boundaries of the studied body from the database, and then to interpolate this new database yielding the regional anomaly map containing all gravity response from the crust, except the one caused by the SAIC (Fig. 9a). This is a more reliable method because it links the anomalies existing on the map with the sources that generate them, as it would have been the same result if SAIC rocks did not exist. After subtracting the regional trend from the Bouguer anomaly map, the result will be a residual map containing only the gravity anomaly related to the body (Fig. 9b), highlighting its gravity response (Ribeiro and Mantovani, 2011).

Residual Bouguer anomaly displayed near-to-zero values out of the expected limits of the granitic body, indicating the effectiveness of the separation. The residual anomaly varied from −3.2 mGal in the SAIC borders up to 14.0 mGal at its southwest mafic core, matching with the inversely zoned rocks (Fig. 2b). The negative anomaly occurred at the borders where the granitic rocks outcrop, especially in the southwest lobe, and becoming positive in the contact with the mixing zone, then assuming the highest values near the exposed area of the mafic cores. The residual map also displays the separation between the two lobes, suggesting the internal shear zone, a lithological and/or volumetric difference of the intrusions. All of them explains the variability in the amplitudes of the anomalies. It is noticeable that the anomalies are slightly skewed, and were interpreted as a southward dip for the southwest mafic core, and a westward dip for the northeast core.

5.3. Shape of the intrusions

5.3.1. Modelling constraints

The modelling constraints were based on the petrophysical properties of the studied rocks. The Henkel plot, which is a cross-plot of the magnetic susceptibility (logarithm scale) against density, reveals two well-marked trends in the petrophysical properties recognized by Henkel (1991) as the "paramagnetic trend" and "ferromagnetic trend". In the Henkel plot using the rock samples from the SAIC and country rocks, shown in the Fig. 10a, it is possible to discern that the majority of the intrusive complex falls in the "ferromagnetic trend", while the country rocks ones (paragneisses and orthogneisses) fall in the "paramagnetic trend". Therefore, the segregation between SAIC rocks and their country rocks due to their petrophysical properties is notorious, with some exceptions of hybrid rock samples falling in the paramagnetic trend and two sites in the orthogneisses (SAG1 and SAG11) with ferromagnetic behavior.

In the density distribution using box-plots (Fig. 10b), it is recognized a similar behavior for the country rocks. On the other hand, the same plot reveals a different distribution of density within the SAIC rocks. Thus, for the sake of simplicity in the modelling process, the country rocks were considered a single entity and the SAIC geology was simplified in two gabbronorite cores, a granitic border and a hybrid zone between them. An average density of 2600 ± 30 kg/m^3 for the border granite was obtained using 57 cylindrical samples. Gabbronorite rocks have a density of 2900 ± 27 kg/m^3, calculated for the mafic cores using 44 samples. Since the degree of hybridization rocks varies in the mixing zone, the density value calculated from 110 samples, of 2780 ± 80 kg/m^3, is intermediate between granitic and gabbronoritic rocks. The standard deviation is higher than those ones obtained from other SAIC rocks, which evidences the heterogeneity of the mixing processes that formed them. Finally, the bulk density of the country rocks was calculated using 152 cylindrical samples, resulting in the averaged value of 2670 ± 60 kg/m^3. The relatively high contrast density between the SAIC and its country rocks gives a good confidence in the modelling of the intrusive complex.

5.3.2. Two-dimensional modelling

The 2D modelling was performed using the selected cross sections with respect of the currently level of erosion, and without vertical exaggeration, drawn parallel and perpendicular to the horizontal elongated axis of the SAIC (Fig. 11). The NW-SE trending profiles (A-A′, B-B′, and C-C′) are perpendicular to the elongated direction of the SAIC and were built on profiles with the highest possible gravity station density, thus being more reliable (see Fig. 2c). Profile A shows the geometry of the southwest lobe, which reaches a maximum thickness around 4 km, and the southward dip (>80°) of the mafic core. Furthermore, the

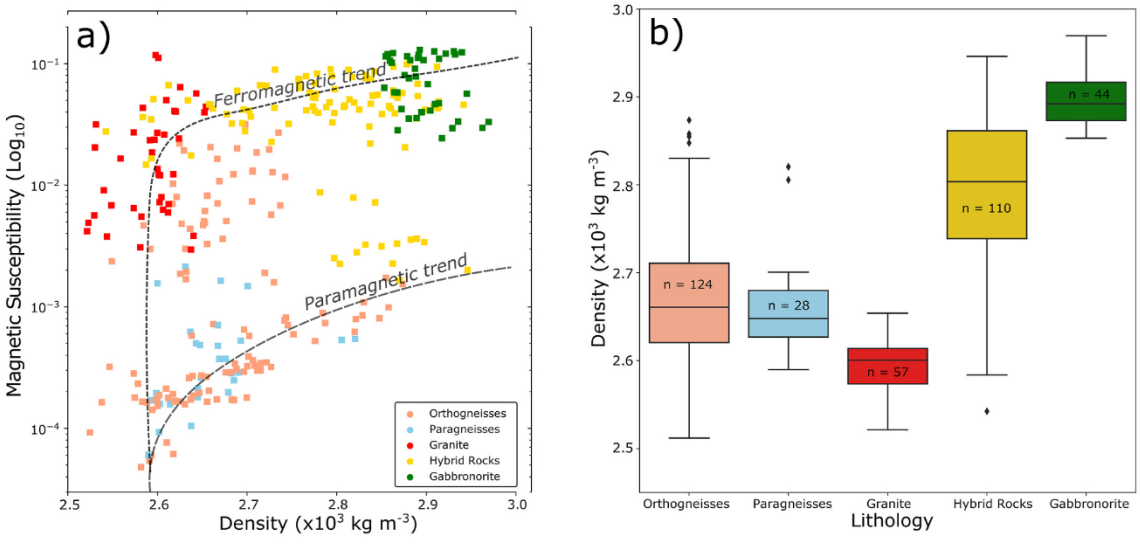

Fig. 10. Petrophysical properties of the studied rocks. (a) Henkel plot showing the well-marked difference in the behavior between the country and the SAIC rocks. (b) Density distribution of the rocks whence it is recognized four density clusters: (i) country rocks; (ii) granitic rocks; (iii) hybrid rocks; and (iv) gabbronorite cores.

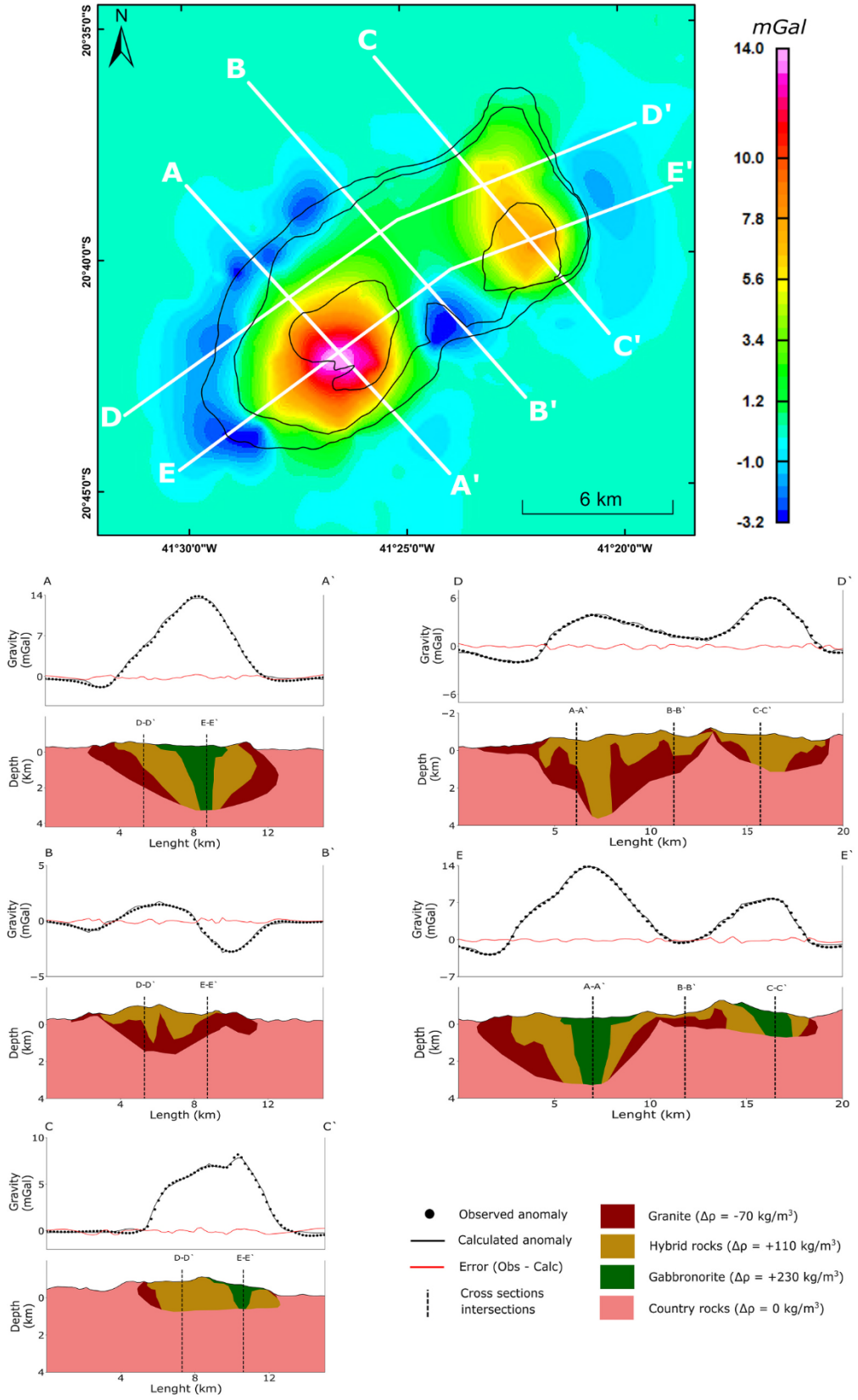

Fig. 11. Residual Bouguer gravity anomaly map for the study area and interpreted profiles of Bouguer gravity anomalies (white line). The thick black lines mark the simplified geological map. The profiles A-A′, B-B′, and C-C′ extend in NW-SE direction, perpendicular to the elongated direction of the SAIC. Profiles D-D′ and E-E′ extend in NE-SW direction, parallel to the SAIC's elongation. The black dots and thin black lines shown in the profiles are plots of measured residual Bouguer gravity anomaly values and the modelling calculated gravity anomalies, respectively, while the thin red lines are the error associated with the modelling. (For interpretation of the references to colour in this figure legend, the reader is referred to the web version of this article.)

positive peak anomaly spatially matches with the southwest lobe's core. The profile B is less thick if compared to the previous profile, and becomes even more shallow when it approaches the SE border, which could be the limit between the two lobes. The profile C provides the geometry of the northeast lobe and a maximum thickness around 2 km. Its maximum anomaly amplitude is smaller than that from the southwest lobe, which results in the thickness difference between them. The NE-SW trending profiles (D-D′ and E-E′) were built parallel to the elongated direction of the SAIC and modelled in order to constrict and respect the previous presented profiles geometry. Profile D also highlights the distinct depths of both lobes, as well as in the profile E, however showing a different position of the facies and the absence of the mafic rocks. The minimum thickness occurs at the location of the internal shear zone.

6. Discussion

6.1. Significance of magnetic fabric and gravity modelling

The presence of ferromagnetic (sensu *lato*) minerals in the country rocks is not always clear from the susceptibility versus temperature (k-T) plot (Fig. 4a-d), some of them show a paramagnetic behavior (low K_m values), although the magnetite (orthogneisses) and pyrrhotite (paragneisses) magnetic transitions are well-marked when applied the first derivative ($\partial k/\partial T$). The magnetic fabric of the majority of country rocks is mainly controlled by the MD magnetite. The geometry of the AMS axes containing the bulk magnetic fabric matches the axes obtained with AARM at low coercivity measurements (Fig. 6), with both techniques yielding very similar orientations. As stated by Temporim et al. (2020a), the same behavior occurs within the SAIC rocks, except that those have higher K_m values of a ferromagnetic fabric. The mineral matrix grain size, observed in the thin-section (Fig. 7), and inferred from FORC diagrams (Fig. 4j,k), seems to become smaller when (i) near the contact between the SAIC and its country rocks, in this case also with the field evidence of sheared rocks (SAG01, Fig. 3a,b) and (ii) within the internal shear zone, which can be another indicator of dynamic deformation causing the comminution of the matrix.

The microstructural evidence found in the granitic border and in the internal shear zone not only shows solid-state dynamic deformation, but also the data provided by Temporim et al. (2020b) show that magnetic lineation is compatible with the dip direction of the magnetic foliation. This same pattern is observed in the country rocks AMS data, meaning that any kinematics would occur almost purely dip-slip and the deformation is related to the emplacement process. Even though the anisotropy degree parameter (P) does not directly reflect the degree of deformation suffered by rocks, in the SAIC rocks this parameter assumes much higher values in rocks where solid-state deformation prevails (Temporim et al. (2020a, 2020b). The country rocks, as expected for a high-grade metamorphic rock, show a large number of solid-state textures, but their P parameter is much lower than the ones found in the SAIC rocks. This is most likely to occur because the value of the P has a positive dependence on the amount of magnetite in the mineral fabric (Rochette et al., 1992), which is more expressive in the SAIC's rocks.

According to Temporim et al. (2020a), the magnetic foliation and lineation within the twin lobes is concentric around the mafic core, but the northeast lobe (Fig. 5d) has magnetic lineation more verticalized when compared to the southeast lobe (Fig. 5c). Both are separated by an internal shear zone, which led an interpretation of the northeastern lobe being closer to the feeder zone (pluton's root) and the southwestern one further away from the root and, therefore, outcropping a shallower portion. This perception is confirmed by the difference in the volumes between the twin lobes, as showed by forward gravity modelling (Fig. 11). The northeast lobe has less than half of the maximum thickness of southwestern one. It is also possible to observe that the internal shear zone area corresponds to limit between the lobes. Evidences like: (i) the wedge-shaped geometry of the lobes, (ii) a maximum thickness occurring near to the cores, and (iii) a concentric pattern are, together, compatible features with the typical post-collisional magmatism with, seemingly, only one central magmatic feeder zone (Petford et al., 2000). The lobes separately display balloon-like shape in map view, compatible with a diapiric emplacement under primordially gravitational stress field (Fowler and Paterson, 1997). We interpreted that these are evidences that the magma buoyancy was the main responsible for SAIC's emplacement.

The country rocks foliation near the SAIC's contact, as described by Schmidt-Thomé and Weber-Diefenbach (1987), is steep and tends to wrap the intrusive complex. This is also observed in the magnetic foliation and, therefore, compatible with the diapiric emplacement model proposed by Bayer et al. (1987). This model explains the concentric foliation by overlapping the regional structures. However, instead of the proposed 1–2 km deformation halo around the SAIC, the magnetic anisotropy data shows a much bigger halo (up to 4 km), where the overlapping and deflection effect fades when increasing the distance from the contact, whereas the regional trend takes place.

6.2. Emplacement of post-collisional plutons and crust rheology

Geothermobarometry method has been widely used in the post-collisional plutons to investigate the emplacement conditions. The southern G5 plutons intruded at pressures corresponding to middle to lower crust levels (~19–30 km) (de Aranda et al., 2020; Ludka and Wiedemann-Leonardos, 2000; Medeiros et al., 2001; de Melo et al., 2020; Mendes et al., 1999; Mendes and de Campos, 2012; Wiedemann et al., 2002). Geophysical data of Assumpção et al. (2013) point out that the southern portion of the AO crust has a current thickness of around 40 km, suggesting that the crust thickness during SAIC emplacement was, at least, 60 km. At such emplacement depth, quartz deforms ductily (Fowler and Paterson, 1997), thus rocks with this mineral in their composition, such as the country rocks, tend to deform more easily when applied a differential force, as the magma buoyancy. Additionally, the AO has been interpreted as a Neoproterozoic example of a hot orogen (Cavalcante et al., 2018; Fossen et al., 2017; Munhá et al., 2005; Petitgirard et al., 2009; Vauchez et al., 2007, 2019) where the middle and the lower crust tend to deform easily. Vauchez et al. (2019) asserted that temperature was around 500 °C during the time of emplacement of SAIC, once AO middle crust had slow cooling rates around 510 to 500 Ma. As a result, the magma ascension through deep crust levels occurs entirely in a ductile field. Therefore, the diapiric mechanism, associated with channeling in weakened deep crust through regional structures (Bayer et al., 1987) is regarded as suitable for the SAIC, and others southern AO post-collisional plutons, magma ascent and emplacement into a ductile crust, yielding an internal concentric decoupled structural pattern (Fig. 12a).

While diapiric magma upwelling is limited by the favorable ductile conditions, the hydrodynamic force caused by the magma buoyance is insufficient to fracture the brittle upper crust due to its colder temperature and high yield strength (Vigneresse, 1995). Unable to keep ascending, the magma spread laterally in the rheological transition brittle-ductile, between tectonic layered of the brittle and cold upper crust and the hot and ductile middle crust, causing a flattening on intrusive bodies of this crustal portion. So, the geometry expected in this case would be a flat-floored pluton. The northern post-collisional plutons in the AO might have experienced this mechanism of emplacement given their large horizontal dimensions, geothermobarometry data compatible with the crust brittle-ductile transition (2.4–3.5 Kbar, Serrano et al., 2018) and the gently dipping foliation and lineation (Angelo et al., 2020; Mondou et al., 2012).

Considering the buoyancy of the magma and the ductile conditions of the crust as important parameters of diapirism mechanism, the continental crust might act as a natural density filter for such intrusions. Mafic magmas would have sufficient buoyancy allowing it to rise through a ductily deformed crust until a limited depth (green area, Fig. 12b). On the other hand, a felsic magma would have the necessary

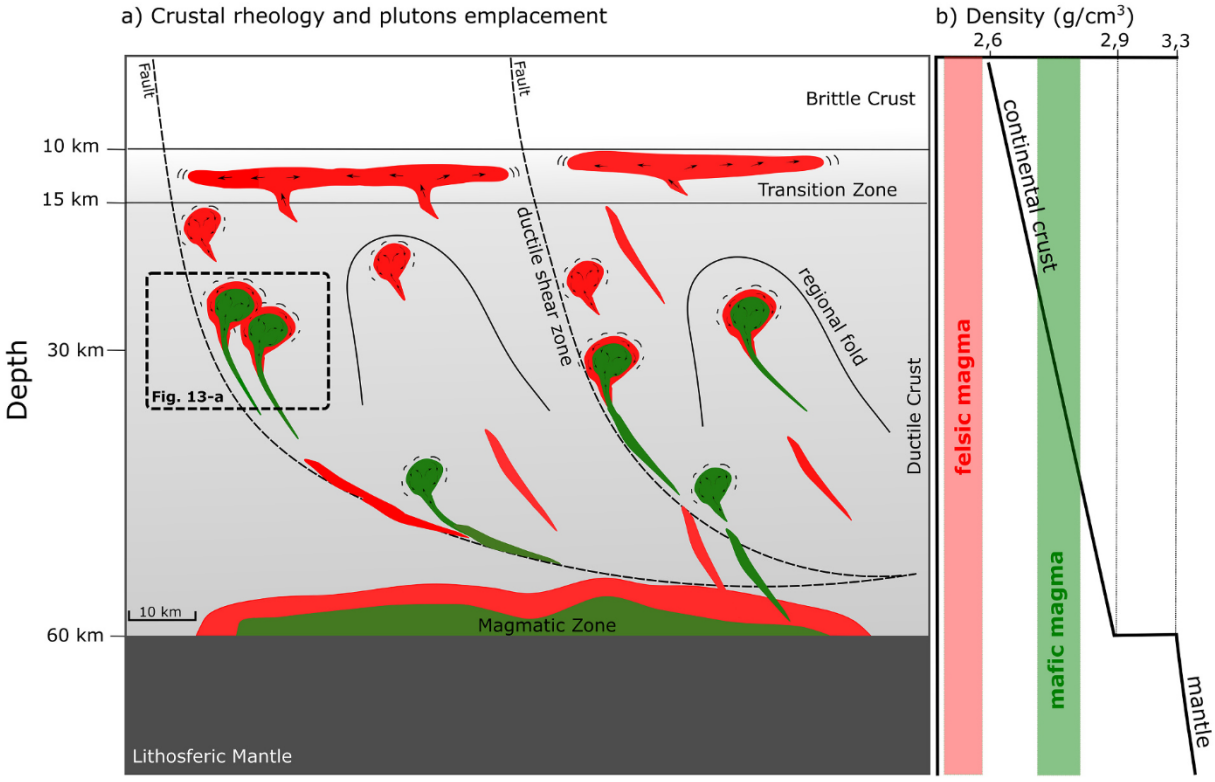

Fig. 12. Simplified scheme showing the emplacement of the G5 supersuite bodies according to the crustal rheology. The green portions represent the mafic magma and the red portions the felsic ones. The black dashes around the balloon-like intrusions in the ductile crust reflects the deformation imparted in the country rocks. Black arrows represent the magma flow. b) Variation in the density of crustal and mantellic rocks, as well as the density intervals of felsic and mafic magmas, as one of the main influencing factors in the depth of plutonic emplacement. (For interpretation of the references to colour in this figure legend, the reader is referred to the web version of this article.)

buoyancy to ascend to the less dense portions of the crust or even the Earth's surface (red area, Fig. 10b), however it is restrained by the cold and rigid limit offered by the upper continental crust, where the diapiric accession mechanism is impractical, provoking lateral spreading.

6.3. *Deformational late stage of post-collisional pluton emplacement*

The physical conditions during the deformation of the final stage of SAIC can be inferred by its microstructures and textures. The distribution of these microstructures suggests a continuous deformational process from the diapiric emplacement (Fig. 13a) to the cooling of the intrusive complex. In the central regions of the complex, where the internal shear zone occurs, microstructures in a submagmatic state are superimposed by high temperature solid state structures. There is no evidence of deformation in the lower temperature solid state overlapping the microstructures mentioned above. This might indicate that deformation ends with the central portion of SAIC still hot, with temperatures around 600–650 °C, but not exceeding this interval once there is absence of ductile deformation in the amphibole (hornblende), whose occurrence requires higher temperatures (Fowler and Paterson, 1997).

The granitic borders generally have the same high temperature microstructures mentioned for the central portion of SAIC. However, there is strong evidence of overlapping by lower temperature microstructures, showing an intermediate efficient recovery process. These microstructures point to a final deformation temperature in these regions between 400 and 500 °C. Finally, the magnetic fabric of the country rocks, deflected by the SAIC intrusion, shows evidence of high temperature deformation, such as the granitic border, but the difference lies in the overlapping of even lower temperature structures, reflecting a temperature range of 350 to 400 °C.

As the magma crystallizes, the proportion of crystals in the melt increases, so that the magma changes from a crystal suspension to a crystal structure, with an interconnected network of pores filled by melting. The submagmatic flow at this stage of crystallization involves a “flow sustained by grains”, as opposed to the magmatic flow, which has “flow of grain suspension” (Vernon, 2000). In other words, the submagmatic flow promotes the deformation of solid minerals, as well as the flow of a small amount of melt. It is very common to occur transitions from submagmatic to solid-state flow through the cooling of igneous bodies during regional deformation (Vernon, 2018). However, the evidence presented by Temporim et al. (2020a) and by this paper, indicates that gravity would be the main driving force during the SAIC emplacement, such as: (i) Zircon U—Pb (SHRIMP) dating coinciding with the post-collisional period of the AO, (ii) the total decoupling of the intrusive complex's internal structure in relation to regional structural geology, and (iii) the overlapping of the deflected structures of the deformational halo in the country rocks related to the emplacement of the SAIC in apparently free from regional tectonic stress conditions.

The continuous deformation from the submagmatic state to the solid-state implies that the granitic border was already crystallized when the mafic cores were cooling, crystallizing and, consequently, becoming denser. As a result, the deformation of both the country rocks and the granitic border, as well as the internal shear zone, was most likely caused by SAIC own negative buoyancy during the crystallization process of its mafic cores (Fig. 13b). Following the mechanism described by Glazner (1994) and Glazner and Miller (1997), as the magma cools and crystallizes, it becomes denser than the surrounding rocks, especially in the case of mafic compositions. Thus, the pluton sinks in the crust if the halo formed in the country rocks (due to the heat emanating during the crystallization process and the of released fluids) is ductile enough to allow the body to move. The emplacement of SAIC in a medium to lower ductile crust of a low cooling rate hot orogen (Vauchez et al., 2019)

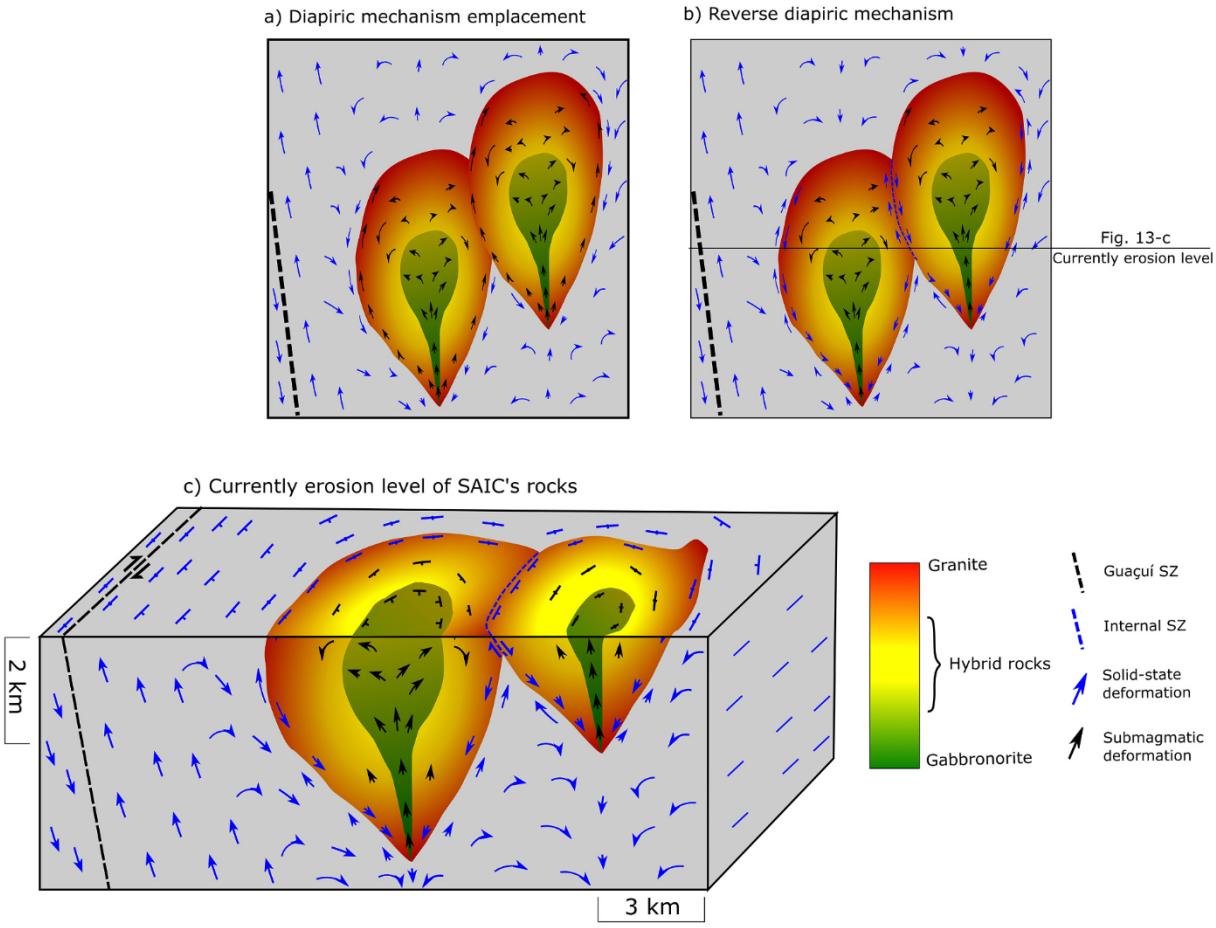

Fig. 13. Schematics of the SAIC emplacement process. a) Diapiric process caused by the buoyancy of magmas. b) Late-emplacement deformation resulting from negative buoyancy, mainly of the mafic cores. c) Current erosion profile based on AMS, gravity and microstructure data.

could easily allow such vertical movement. Paterson and Tobisch (1988) and Miller and Paterson (1994) conclude that the continuous deformation during the cooling process of the pluton occurs when it intrudes in crustal levels that allows the cooling in a slow way, which agrees with our interpretation. Such a slow cooling rate is described for the AO by Vauchez et al. (2019). This process ends when the halo cools down, or, when the body reaches a level with denser and/or more resistant rocks. The first cause is the most likely to occur due to the high lateral contrast of density and the low-temperature microstructures observed in the country rocks.

The proposed mechanism can explain why SAIC is the only example in the southern portion of the AO with an expressive amount of solid-state deformation at the granitic edges (and in the internal shear zone) and the preservation of submagmatic features in the hybrid rock zone and in the core. The kinematics of the internal shear zone, with ENE dip direction and normal movement (*normal dip-slip*), showed that the northeast lobe sinks when compared to the southwest (Fig. 13c). However, apparently, both would sink when compared to the country rocks, although we did not find conclusive kinematic indicators for such statement.

Such specific geological distribution of mafic core (and hybrid rocks) surrounded by coarse-grained porphyritic granitic ring with, and concentric pattern contact with the country rocks is also observed in late-orogenic, or post-kinematics, Vrådal pluton - southern Norway (Sylvester, 1964). The emplacement of this specific pluton described by Sylvester (1998) as a late-stage sinking, that provoked the downbending of the wall-rocks and obliteration of its early formed structures, is supported by the high density of the mafic and hybrid rocks in comparison with the country rocks and the rare structural evidence of upward rise. Another contrasting example of inversely zoned body is the Toro pluton, which is an annular intrusion with a diorite core and a granitic ring that intrudes granites, gneisses and migmatites located in the mobile belt of Central Africa (Nigeria) (Déléris et al., 1996). Its internal structure was investigated by AMS and microstructural data by Déléris et al. (1996), and some of the key points of their interpretation are: (i) a granitic magma first emplaces acquiring a concentric foliation pattern and submagmatic fabric, (ii) dioritic magmas intrude before full-crystallization of the granites re-heating the granites and acquiring a concentric magmatic fabric; and (iii) the granitic fabric is later overprinted by a solid-state structure mostly concordant with the country rocks, while the mafic core preserved its concentric submagmatic pattern, pointing out that the Toro is a syntectonic pluton with a partition deformation concentrated in the borders. Understanding such contrasting mechanisms of magma accommodation under tectonic conditions in the Vrådal and Toro plutons might be essential to insight the SAIC's emplacement model, since they all share similar geological features, but the SAIC rocks structural data seems more coherent with the Vrådal pluton.

7. Conclusions

SAIC is one of the most representative bodies of the G5 supersuite, which is an example of the Ediacaran-Cambrian (530–480 Ma) post-collisional magmatism of the AO. Outcropping in the southern and deeper portion of the Araçuaí Orogen, the SAIC, as well as other synchronous intrusions from the same region, is a balloon-like pluton with an inverse concentric zoning, with mafic rocks in the central portion

grading to more felsic ones at the borders. However, unlike other southern bodies, the SAIC granitic border has stronger evidence of solid-state deformation, as well as in its internal shear zone. The borders of SAIC rocks and its country rocks register continuous solid-deformation features (i.e., from high to low temperatures), meanwhile, the internal shear zone only register high temperature solid-state deformational features.

The interpretation of the magnetic characterization of the SAIC's country rocks lead to the following remarks: (i) magnetite is the main magnetic phase in the orthogneisses samples, as evidenced by Verwey and Curie characteristic magnetic transitions, obtained from the thermomagnetic curves and the pyrrhotite is dominant ferromagnetic phase in the paragneisses; (ii) hysteresis loops, IRMs and FORCs analysis suggest that the magnetic carriers in the sheared contact with SAIC rocks ranges in the PSD-spectrum, while country rocks samples without shear deformation evidences tend to fall in the MD range; (iii) low values of K_m suggests fabric behavior mainly controlled by paramagnetic minerals, however; (iv) ASM data is showed to be mainly controlled by MD magnetite, as proved by the integration of AARM data; and (v) the magnetic fabric of the country rocks on the border parallel to the contact direction of SAIC overlaps the regional trend and the influence of the Guaçuí shear zone, thus, compatible with the diapiric emplacement model.

The residual gravity data reflected the local geological variation, individualizing both the southwest and northeast lobes, and the shear zone between them. The SAIC modelled lobes corroborated with the AMS data, with the northeast lobe (less thick) closer to the magma feeder zone than the southwest lobe. It suggested that the minimum thickness of the complex occurs within the internal shear zone, which marks the contact zone between the twin plutons. The ASM concentric pattern around the mafic cores associated with the intrusion geometry also suggests the presence of only one, or few, magma feeder channel for each lobe.

The integration of these results allowed us to infer that the late deformation stage might have occurred due to a mechanism of reverse diapirism. Such was probably caused by the negative buoyance forces generated by crystallizing the mafic cores, which sink through a hot ductile halo in the crust, yielding all the solid-state meso-microstructures and the normal dip-slip kinematics of the internal shear zone. This mechanism could only occur in the deep and hot crust, where the inversely zoned plutons are formed. Meanwhile, we argue that a shallower midcrust would work as a natural density filter zone, only allowing felsic magmas to arise. Once they reach the brittle/ductile rheological zone, the diapiric mechanism is no longer effective to allow further ascension, so it spreads horizontally instead, which reflects the large post-collisional batholiths with sub-horizontal fabric in the northern AO. The geophysical observations applied to investigate the geometry in depth of intrusive bodies and the insight of mechanisms of magma emplacement, and deformation, have often been used to designate their displayed architectures. We have shown that the inverse diapiric mechanism is also suitable and recognized in others examples around the world, as well as the difference between the deformation during a syn and post-kinematic phases. Our study shows how buoyance of the mafic and felsic magmas, together with crustal rheology, might constitute constraints responsible to restrain the emplacement depth and geometry of post-collisional plutons.

Declaration of Competing Interest

The authors declare that they have no known competing financial interests or personal relationships that could have appeared to influence the work reported in this paper.

Acknowledges

The authors would like to express their gratitude to Yara R. Marangoni for her support in the acquisition of the regional gravity database as well as the Banco Nacional de Dados Gravimétricos (BNDG) for providing this database; to Roberto P. Zanon do Santos for his support in the acquisition of the gravity data during field work. The infrastructure and collaborations of the Laboratório de Paleomagnetismo of the Universidade de São Paulo (USPMag). This work was funded by grants of Fundação de Amparo à Pesquisa do Estado de São Paulo (FAPESP, Research Foundation Project #2016/06114-6) and the Coordenação de Aperfeiçoamento de Pessoal de Nível Superior (CAPES). We also would like to thank Zheng-Xiang Li, Silvana Geuna and an anonymous reviewer for their critical reviews that certainly helped to improve the quality of this paper.

References

Alkmim, F.F., Marshak, S., Pedrosa-Soares, A.C., Peres, G.G., Cruz, S.C.P., Whittington, A., 2006. Kinematic evolution of the Araçuaí-West Congo orogen in Brazil and Africa: nutcracker tectonics during the Neoproterozoic assembly of Gondwana. Precambrian Res. 149 (1–2), 43–64. https://doi.org/10.1016/j.precamres.2006.06.007.

Alkmim, F.F., Pedrosa-Soares, A.C., Noce, C.M., Cruz, S.C.P., 2007. Sobre a Evolução Tectônica do Orógeno Araçuaí-Congo Ocidental. Geonomos 15, 25–43. https://doi.org/10.18285/geonomos.v15i1.105.

Améglio, L., Vigneresse, J.L., 1999. Geophysical imaging of the shape of granitic intrusions at depth: a review. Geol. Soc. Spec. Publ. 168 (1), 39–54. https://doi.org/10.1144/GSL.SP.1999.168.01.04.

Améglio, L., Vigneresse, J.L., Bouchez, J.L., 1997. Granite pluton geometry and emplacement mode inferred from combined fabric and gravity data. In: Granite: From Segregation of Melt to Emplacement Fabrics, vol. 8. Springer, Dordrecht, pp. 199–214. https://doi.org/10.1007/978-94-017-1717-5_13.

Angelo, T.V., Egydio-Silva, M., Temporim, F.A., Seraine, M., 2020. Midcrust deformation regime variations across the Neoproterozoic Araçuaí hot orogen (SE Brazil): insights from structural and magnetic fabric analyses. J. Struct. Geol. 134, 104007 https://doi.org/10.1016/j.jsg.2020.104007.

Araujo, C., Pedrosa-Soares, A., Lana, C., Dussin, I., Queiroga, G., Serrano, P., Medeiros-Júnior, E., 2020. Zircon in emplacement borders of post-collisional plutons compared to country rocks: a study on morphology, internal texture, U–Th–Pb geochronology and Hf isotopes (Araçuaí orogen, SE Brazil). Lithos 352–353, 105252. https://doi.org/10.1016/j.lithos.2019.105252.

Archanjo, C.J., Launeau, P., Bouchez, J.L., 1995. Magnetic fabric vs. magnetite and biotite shape fabrics of the magnetite-bearing granite pluton of Gameleiras (Northeast Brazil). Phys. Earth Planet. Inter. 89 (1–2), 63–75. https://doi.org/10.1016/0031-9201(94)02997-P.

Arzi, A.A., 1978. Critical phenomena in the rheology of partially melted rocks. Tectonophysics 44 (1–4), 173–184. https://doi.org/10.1016/0040-1951(78)90069-0.

Assumpção, M., Bianchi, M., Julià, J., Dias, F.L., Sand França, G., Nascimento, R., Drouet, S., Pavão, C.G., Albuquerque, D.F., Lopes, A.E.V., 2013. Crustal thickness map of Brazil: data compilation and main features. J. S. Am. Earth Sci. 43, 74–85. https://doi.org/10.1016/j.jsames.2012.12.009.

Bayer, P., Schmidt-Thomé, R., Weber-Diefenbach, K., Horn, H.A., 1987. Complex concentric granitoid intrusions in the coastal mobile belt, Espírito Santo, Brazil: the Santa Angélica Pluton - an example. Geol. Rundsch. 76 (2), 357–371. https://doi.org/10.1007/BF01821080.

Bellon, U.D., D'Agrella-Filho, M.S., Temporim, F.A., Souza Junior, G.F., Soares, C.C.V., Amaral, C.A.D., Gouvêa, L.P., Trindade, R.I.F., 2021. Building an inversely zoned post-orogenic intrusion in the Neoproterozoic-Cambrian Araçuaí orogen (Brazil). J. Struct. Geol. 149 (February), 104401 https://doi.org/10.1016/j.jsg.2021.104401.

Blumenfeld, P., Bouchez, J.L., 1988. Shear criteria in granite and migmatite deformed in the magmatic and solid states. J. Struct. Geol. 10 (4), 361–372. https://doi.org/10.1016/0191-8141(88)90014-4.

Bouchez, J.L., 1997. Granite is never isotropic: an introduction to AMS studies of granitic rocks. In: Bouchez, J.L., Hutton, D.H.W., Stephens, W.E. (Eds.), Granite : From Segregation of Melt to Emplacement Fabrics. Kluwer Academic Publishers, Dordrecht, pp. 95–112. https://doi.org/10.1007/978-94-017-1717-5_6.

Bouchez, J.L., Gleizes, G., Djouadi, T., Rochette, P., 1990. Microstructure and magnetic susceptibility applied to emplacement kinematics of granites: the example of the foix pluton (French pyrenees). Tectonophysics 184 (2), 157–171. https://doi.org/10.1016/0040-1951(90)90051-9.

Bouchez, J.L., Delas, C., Gleizes, G., Nedelec, A., Cuney, M., 1992. Submagmatic microfractures in granites. Geology 20 (1), 35–38. https://doi.org/10.1130/0091-7613(1992)020<0035:SMIG>2.3.CO;2.

Cavalcante, C., Hollanda, M.H., Vauchez, A., Kawata, M., 2018. How long can the middle crust remain partially molten during orogeny? Geology 46 (10), 839–842. https://doi.org/10.1130/G45126.1.

Chapin, D.A., 1996. The theory of the Bouguer gravity anomaly: a tutorial. Leading Edge (Tulsa, OK) 15 (5), 361. https://doi.org/10.1190/1.1437341.

Collinson, D.W., 1983. Methods in Rock Magnetism and Palaeomagnetism: Techniques and Instrumentation. Chapman & Hall, London.

Da Silva, L.C., McNaughton, N.J., Armstrong, R., Hartmann, L.A., Fletcher, I.R., 2005. The neoproterozoic Mantiqueira Province and its African connections: a zircon-based U-Pb geochronologic subdivision for the Brasiliano/Pan-African systems of

orogens. Precambrian Res. 136 (3–4), 203–240. https://doi.org/10.1016/j.precamres.2004.10.004.
Day, R., Fuller, M., Schmidt, V.A., 1977. Hysteresis properties of titanomagnetites: grain-size and compositional dependence. Phys. Earth Planet. Inter. 13 (4), 260–267. https://doi.org/10.1016/0031-9201(77)90108-X.
de Aranda, R.O., Horn, A.H., de Medeiros Júnior, E.B., Venturini Junior, R., 2020. Geothermobarometry of igneous rocks from Afonso Cláudio Intrusive Complex (Espírito Santo state, Southeastern Brazil), Arauaí-West Congo Orogen: further evidence for deep emplacement levels. J. S. Am. Earth Sci. 16 https://doi.org/10.1016/j.jsames.2020.103016.
De Campos, C.M.P., Mendes, J.C., Ludka, I.P., 2004. A review of the Brasiliano magmatism in southern Espírito Santo, Brazil, with emphasis on postcollisional magmatism. J. Virtual Explor. 17, 1–39. https://doi.org/10.3809/jvirtex.2004.00106.
De Campos, C.M.P., de Medeiros, S.R., Mendes, J.C., Pedrosa-Soares, A.C., Dussin, I., Ludka, I.P., Dantas, E.L., 2016. Cambro-Ordovician magmatism in the Araçuaí Belt (SE Brazil): snapshots from a post-collisional event. J. S. Am. Earth Sci. 68, 248–268. https://doi.org/10.1016/j.jsames.2015.11.016.
de Melo, M.G., Lana, C., Stevens, G., Hartwig, M.E., Pimenta, M.S., Nalini, H.A., 2020. Deciphering the source of multiple U–Pb ages and complex Hf isotope composition in zircon from post-collisional charnockite-granite associations from the Araçuaí orogen (southeastern Brazil). J. S. Am. Earth Sci. 103, 102792 https://doi.org/10.1016/j.jsames.2020.102792.
Déléris, J., Nédélec, A., Ferré, E., Gleizes, G.R., Ménot, R., 1996. The Pan-African Toro Complex northern Nigeria: magmatic interactions and structures in a bimodal intrusion. Geol. Mag. 133 (5), 535–552. https://doi.org/10.1017/S0016756800007822.
Dunlop, D.J., Özdemir, Ö., 1997. Rock magnetism fundamentals and frontiers. In: Rock Magnetism. Cambridge University Press. https://doi.org/10.1017/cbo9780511612794.
Fossen, H., Cavalcante, G.C., Almeida, R.P., 2017. Hot versus cold orogenic behavior: comparing the Araçuaí-West Congo and the Caledonian Orogens. Tectonics 36 (10), 2159–2178. https://doi.org/10.1002/2017TC004743.
Fossen, H., Cavalcante, C., Konopásek, J., Meira, V.T., de Almeida, R.P., Hollanda, M.H. B.M., Trompette, R., 2020. A critical discussion of the subduction-collision model for the Neoproterozoic Araçuaí-West Congo orogen. Precambr. Res. 343 https://doi.org/10.1016/j.precamres.2020.105715.
Fowler, T.K., Paterson, S.R., 1997. Timing and nature of magmatic fabrics from structural relations around stoped blocks. J. Struct. Geol. 19 (2), 209–224. https://doi.org/10.1016/S0191-8141(96)00058-2.
Glazner, A.F., 1994. Foundering of mafic plutons and density stratification of continental crust. Geology 22 (5), 435–438. https://doi.org/10.1130/0091-7613(1994)022<0435:FOMPAD>2.3.CO;2.
Glazner, A.F., Miller, D.M., 1997. Late-stage sinking of plutons. Geology 25 (12), 1099–1102. https://doi.org/10.1130/0091-7613(1997)025<1099:LSSOP>2.3.CO;2.
Henkel, H., 1991. Petrophysical properties (density and magnetization) of rocks from the northern part of the Baltic Shield. Tectonophysics 192 (1–2), 1–19. https://doi.org/10.1016/0040-1951(91)90242-K.
Hrouda, F., 1982. Magnetic anisotropy of rocks and its application in geology and geophysics. Geophys. Surv. 5 (1), 37–82. https://doi.org/10.1007/BF01450244.
Jackson, M., 1991. Anisotropy of magnetic remanence: a brief review of mineralogical sources, physical origins, and geological applications, and comparison with susceptibility anisotropy. Pure Appl. Geophys. 136 (1), 1–28. https://doi.org/10.1007/BF00878885.
Jelínek, V., 1978. Statistical processing of anisotropy of magnetic susceptibility measured on groups of specimens. Stud. Geophys. Geod. 22 (1), 50–62. https://doi.org/10.1007/BF01613632.
Lowrie, W., 1997. Fundamental of Geophysics. Cambridge University Press.
Ludka, I.P., Wiedemann-Leonardos, C.M., 2000. Further signs of an enriched mantle source under the neoproterozoic Araçuaí-Ribeira Mobile Belt. Rev. Brasil. Geoci. 30, 95–98.
Medeiros, S.R., Wiedemann-Leonardos, C.M.P., Vriend, S., 2001. Evidence of mingling between contrasting magmas in a deep plutonic environment: the example of Várzea Alegre, in the Ribeira Mobile Belt, Espírito Santo, Brazil. Anais Acad. Brasil. Cien. 73 (1), 99–119. https://doi.org/10.1590/S0001-37652001000100009.
Mendes, J.C., de Campos, C.P., 2012. Norite and charnockites from the Venda Nova Pluton, SE Brazil: intensive parameters and some petrogenetic constraints. Geosci. Front. 3 (6), 789–800. https://doi.org/10.1016/j.gsf.2012.05.009.
Mendes, J.C., Wiedemann, C.M.P., McReath, I., 1999. Conditions of formation of charnockitic magmatic rocks from the V'arzea Alegre massif, Espírito Santo, southeastern Brazil. Rev. Brasil. Geoci. 29, 47–57. https://doi.org/10.25249/0375-7536.1999294754.
Miller, R.B., Paterson, S.R., 1994. The transition from magmatic to high-temperature solid-state deformation: implications from the Mount Stuart batholith, Washington. J. Struct. Geol. 16 (6), 853–865. https://doi.org/10.1016/0191-8141(94)90150-3.
Mondou, M., Egydio-Silva, M., Vauchez, A., Raposo, M.I.B., Bruguier, O., Oliveira, A.F., 2012. Complex, 3D strain patterns in a synkinematic tonalite batholith from the Araçuaí Neoproterozoic orogen (Eastern Brazil): evidence from combined magnetic and isotopic chronology studies. J. Struct. Geol. 39, 158–179. https://doi.org/10.1016/J.JSG.2012.02.015.
Munhá, J.M.U., Cordani, U., Tassinari, C.C.G., Palácios, T., 2005. Petrologia e termocronologia de gnaisses migmatíticos da Faixa de Dobramentos Araçuaí (Espírito Santo, Brasil). Rev. Brasil. Geoci. 35, 123–134. http://www.ppegeo.igc.usp.br/index.php/rbg/article/viewFile/9774/9711.
Nagata, T., 1961. Rock Magnetism. Maruzen, Tokyo.
Passchier, C.W., Trouw, R.A.J., 2005. Microtectonics. In: Passchier, C.W., Trouw, R.A.J. (Eds.), Microtectonics, 2nd ed. Springer. https://doi.org/10.1007/3-540-29359-0_3.
Paterson, S.R., Tobisch, O.T., 1988. Using pluton ages to date regional deformations: problems with commonly used criteria. Geology 16 (12), 1108–1111. https://doi.org/10.1130/0091-7613(1988)016<1108:UPATDR>2.3.CO;2.
Paterson, S.R., Vernon, R.H., Tobisch, O.T., 1989. A review of criteria for the identification of magmatic and tectonic foliations in granitoids. J. Struct. Geol. 11 (3), 349–363. https://doi.org/10.1016/0191-8141(89)90074-6.
Paterson, S.R., Fowler, T.K., Schmidt, K.L., Yoshinobu, A.S., Yuan, E.S., Miller, R.B., 1998. Interpreting magmatic fabric patterns in plutons. Lithos 44 (1–2), 53–82. https://doi.org/10.1016/S0024-4937(98)00022-X.
Pedrosa-Soares, A.C., Wiedemann-Leonardos, C.M., 2000. Evolution of the Araçuaí Belt and its connection to the Ribeira Belt, Eastern Brazil. In: Cordani, U.G., Milani, E.J., Thomaz Filho, A., Campos, D.A. (Eds.), Tectonic Evolution of South America. SBG, pp. 265–285. https://www.researchgate.net/publication/303241376_Evolution_of_the_Aracuai_Belt_and_its_connection_to_the_Ribeira_Belt_Eastern_Brazil.
Pedrosa-Soares, A.C., Alkmim, F.F., Tack, L., Noce, C.M., Babinski, M., Silva, L.C., Martins-Neto, M.A., 2008. Similarities and differences between the Brazilian and African counterparts of the Neoproterozoic Araçuaí-West Congo Orogen. Geol. Soc. Spec. Publ. 294 (1), 153–172. https://doi.org/10.1144/SP294.9.
Pedrosa-Soares, A.C., de Campos, C.M.P., Noce, C., Silva, L.C., Novo, T., Roncato, J., Medeiros, S., Castañeda, C., Queiroga, G., Dantas, E., Dussin, I., Alkmim, F., 2011. Late Neoproterozoic-Cambrian granitic magmatism in the Araçuaí orogen (Brazil), the Eastern Brazilian Pegmatite Province and related mineral resources. Geol. Soc. Spec. Publ. 350 (1), 25–51. https://doi.org/10.1144/SP350.3.
Petford, N., Cruden, A.R., McCaffrey, K.J.W., Vigneresse, J.L., 2000. Granite magma formation, transport and emplacement in the Earth's crust. Nature 408 (6813), 669–673. https://doi.org/10.1038/35047000.
Petitgirard, S., Vauchez, A., Egydio-Silva, M., Bruguier, O., Camps, P., Monié, P., Babinski, M., Mondou, M., 2009. Conflicting structural and geochronological data from the Ibituruna quartz-syenite (SE Brazil): effect of protracted "hot" orogeny and slow cooling rate? Tectonophysics 477 (3–4), 174–196. https://doi.org/10.1016/j.tecto.2009.02.039.
Ribeiro, V.B., Mantovani, M.S.M., 2011. Campo gravimétrico do complexo alcalino de tapira (MG): comparação entre técnicas de interpolação e de separação regional-residual. Rev. Brasil. Geofis. 29 (3), 463–485. https://doi.org/10.22564/rbgf.v29i3.93.
Roberts, A.P., Pike, C.R., Verosub, K.L., 2000. First-order reversal curve diagrams: a new tool for characterizing the magnetic properties of natural samples. J. Geophys. Res. 105 (B12), 28461–28475. https://doi.org/10.1029/2000JB900326.
Rochette, P., 1987. Magnetic susceptibility of the rock matrix related to magnetic fabric studies. J. Struct. Geol. 9 (8), 1015–1020. https://doi.org/10.1016/0191-8141(87)90009-5.
Rochette, P., Jackson, M., Aubourg, C., 1992. Rock magnetism and the interpretation of anisotropy of magnetic susceptibility. Rev. Geophys. 30 (3), 209–226. https://doi.org/10.1029/92RG00733.
Schmidt-Thomé, R., Weber-Diefenbach, K., 1987. Evidence for" frozen-in" magma mixing in Brasiliano calc-alkaline intrusions: the Santa Angelica pluton, southern Espírito Santo, Brazil. Rev. Brasil. Geoci. 17 (4), 498–506. http://www.ppegeo.igc.usp.br/index.php/rbg/article/view/11962.
Serrano, P., Pedrosa-Soares, A., Medeiros-Júnior, E., Fonte-Boa, T., Araujo, C., Dussin, I., Queiroga, G., Lana, C., 2018. A-type Medina batholith and post-collisional anatexis in the Araçuaí orogen (SE Brazil). Lithos 320–321, 515–536. https://doi.org/10.1016/j.lithos.2018.09.009.
Silva, C.M.T., 2010. O Sistema Transcorrente da Porção Sudeste do Orógeno Araçuaí e Norte da Faixa Ribeira: Geometria e Significado Tectônico. Programa de Pós-Graduação em Evolução Crustal e Recursos Naturais. Departamento de Geologia.
Stipp, M., Stünitz, H., Heilbronner, R., Schmid, S.M., 2002. The eastern Tonale fault zone: a "natural laboratory" for crystal plastic deformation of quartz over a temperature range from 250 to 700 °C. J. Struct. Geol. 24 (12), 1861–1884. https://doi.org/10.1016/S0191-8141(02)00035-4.
Sylvester, A.G., 1964. The Precambrian rocks of the Telemark area in south central Norway. III Geology of the Vrådal granite. Nor. Geol. Tidsskr. 44, 445–482.
Sylvester, A.G., 1998. Magma mixing, structure, and re-evaluation of the emplacement mechanism of Vrådal pluton, central Telemark, southem Norway. Nor. Geol. Tidsskr. 78, 259–276.
Talwani, M., Worzel, J.L., Landisman, M., 1959. Rapid gravity computations for two-dimensional bodies with application to the Mendocino submarine fracture zone. J. Geophys. Res. 64 (1), 49–59. https://doi.org/10.1029/jz064i001p00049.
Telford, W.M., Geldart, L.P., Sheriff, R.E., 1990. Applied geophysics, 2nd ed. Cambridge University Press, UK.
Temporim, F.A., Trindade, R.I.F., Tohver, E., Soares, C.C., Gouvêa, L.P., Egydio-Silva, M., Amaral, C.A.D., Souza Junior, G.F., 2020a. Magnetic fabric and geochronology of a Cambrian "Isotropic" Pluton in the Neoproterozoic Araçuaí Orogen. Tectonics 39 (6). https://doi.org/10.1029/2019TC005877.
Temporim, F.A., Trindade, R., Tohver, E., Soares, C., Gouvêa, L.P., Egydio-Silva, M., Amaral, C., Souza Jr., G., 2020b. AMS Data of the Santa Angélica Pluton, p. 2. https://doi.org/10.17632/3XTH2S5CP9.2.
Trindade, R.I.F., Bouchez, J.L., Bolle, O., Nédélec, A., Peschler, A., Poitrasson, F., 2001. Secondary fabrics revealed by remanence anisotropy: methodological study and examples from plutonic rocks. Geophys. J. Int. 147 (2), 310–318. https://doi.org/10.1046/j.0956-540X.2001.01529.x.
Vauchez, Alain, Egydio-Silva, M., Babinski, M., Tommasi, A., Uhlein, A., Liu, D., 2007. Deformation of a pervasively molten middle crust: insights from the neoproterozoic Ribeira-Araçuaí orogen (SE Brazil). Terra Nova 19 (4), 278–286. https://doi.org/10.1111/j.1365-3121.2007.00747.x.

Vauchez, A., Hollanda, M.H.B.M., Monié, P., Mondou, M., Egydio-Silva, M., 2019. Slow cooling and crystallization of the roots of the Neoproterozoic Araçuaí hot orogen (SE Brazil): implications for rheology, strain distribution, and deformation analysis. Tectonophysics 766, 500–518. https://doi.org/10.1016/j.tecto.2019.05.013.

Vernon, R.H., 1988. Microstructural evidence of rotation and non-rotation of mica porphyroblasts. J. Metamorph. Geol. 6 (5), 595–601. https://doi.org/10.1111/j.1525-1314.1988.tb00442.x.

Vernon, R.H., 2000. Review of microstructural evidence of magmatic and solid-state flow. Electron. Geosci. 5 (2), 1–23. https://doi.org/10.1007/s10069-000-0002-3.

Vernon, R.H., 2018. Microstructures of Deformed Rocks. In: A Pratical Guide to Rock Microstructure. Cambridge University Press, pp. 228–352. https://doi.org/10.1017/9781108654609.007. Issues 8–9.

Vernon, R.H., Williams, V.A., D'arcy, W.F., 1983. Grain-size reduction and foliation development in a deformed granitoid Batholith. Tectonophysics 92 (1–3), 123–145. https://doi.org/10.1016/0040-1951(83)90087-2.

Vigneresse, J.L., 1995. Crustal regime of deformation and ascent of granitic magma. Tectonophysics 249 (3–4), 187–202. https://doi.org/10.1016/0040-1951(95)00005-8.

Vigneresse, J.L., Tikoff, B., Améglio, L., 1999. Modification of the regional stress field by magma intrusion and formation of tabular granitic plutons. Tectonophysics 302 (3–4), 203–224. https://doi.org/10.1016/S0040-1951(98)00285-6.

Wiedemann, C.M.P., De Medeiros, S.R., Ludka, I.P., Mendes, J.C., Costa-de-Moura, J., 2002. Architecture of Late Orogenic Plutons in the Araçuaí-Ribeira Fold Belt, Southeast Brazil. Gondwana Res. 5 (2), 381–399. https://doi.org/10.1016/S1342-937X(05)70730-9.

Wiedemann-Leonardos, C.M.P., Ludka, I.P., De Medeiros, S.R., Mendes, J.C., Costa-De-Moura, J., 2000. Arquitetura de Plutons Zonados da Faixa Araçuaí-Ribeira. Geonomos 15 (1), 25–38.